Article

Current Biology

Interactions between pili affect the outcome of bacterial competition driven by the type VI secretion system

Highlights

- Type IV pili facilitate type VI secretion system-mediated killing in liquid
- Natural variation in major pilins and T6SS effector/immunity proteins is explored
- Autoaggregation via matching type IV pili protects closely related individuals from T6SS assaults
- Modeling shows that spatial assortment and lysis time are key for T6SS efficiency

Authors

Simon B. Otto, Richard Servajean, Alexandre Lemopoulos, Anne-Florence Bitbol, Melanie Blokesch

Correspondence

melanie.blokesch@epfl.ch

In brief

Otto et al. explore the interaction between type IV pili (T4Ps) and the type VI secretion system (T6SS) in *Vibrio cholerae*. They find that T4Ps enhance T6SS's lethal efficiency in liquid environments and that diversity within T4P components modulates bacterial competition intensity. Thus, T4Ps can shape the competitive landscape driven by T6SS activities.

Otto et al., 2024, Current Biology *34*, 1–15
June 3, 2024
https://doi.org/10.1016/j.cub.2024.04.041

CellPress

Current Biology

CellPress
OPEN ACCESS

Article

Interactions between pili affect the outcome of bacterial competition driven by the type VI secretion system

Simon B. Otto,[1] Richard Servajean,[2,3] Alexandre Lemopoulos,[1] Anne-Florence Bitbol,[2,3] and Melanie Blokesch[1,4,5,*]
[1]Laboratory of Molecular Microbiology, Global Health Institute, School of Life Sciences, École Polytechnique Fédérale de Lausanne (EPFL), 1015 Lausanne, Switzerland
[2]Laboratory of Computational Biology and Theoretical Biophysics, Institute of Bioengineering, School of Life Sciences, École Polytechnique Fédérale de Lausanne (EPFL), 1015 Lausanne, Switzerland
[3]SIB Swiss Institute of Bioinformatics, 1015 Lausanne, Switzerland
[4]X (formerly Twitter): @MBlokesch
[5]Lead contact
*Correspondence: melanie.blokesch@epfl.ch
https://doi.org/10.1016/j.cub.2024.04.041

SUMMARY

The bacterial type VI secretion system (T6SS) is a widespread, kin-discriminatory weapon capable of shaping microbial communities. Due to the system's dependency on contact, cellular interactions can lead to either competition or kin protection. Cell-to-cell contact is often accomplished via surface-exposed type IV pili (T4Ps). In *Vibrio cholerae*, these T4Ps facilitate specific interactions when the bacteria colonize natural chitinous surfaces. However, it has remained unclear whether and, if so, how these interactions affect the bacterium's T6SS-mediated killing. In this study, we demonstrate that pilus-mediated interactions can be harnessed by T6SS-equipped *V. cholerae* to kill non-kin cells under liquid growth conditions. We also show that the naturally occurring diversity of pili determines the likelihood of cell-to-cell contact and, consequently, the extent of T6SS-mediated competition. To determine the factors that enable or hinder the T6SS's targeted reduction of competitors carrying pili, we developed a physics-grounded computational model for autoaggregation. Collectively, our research demonstrates that T4Ps involved in cell-to-cell contact can impose a selective burden when *V. cholerae* encounters non-kin cells that possess an active T6SS. Additionally, our study underscores the significance of T4P diversity in protecting closely related individuals from T6SS attacks through autoaggregation and spatial segregation.

INTRODUCTION

The composition of microbial populations has a significant impact on ecological functions and host health.[1,2] Interbacterial interactions are often antagonistic in nature and target closely related species, ultimately influencing microbial populations by aiding in niche colonization and exclusion.[3–5] In order to achieve this, bacteria possess a myriad of weapons and defense mechanisms.[6] Interactions between species can be achieved through two primary mechanisms: the release of diffusible compounds and contact-dependent interactions.[7,8] Unlike diffusible compounds, which can disperse into the surrounding environment, contact-dependent mechanisms require direct cell-to-cell interaction to effectively deliver toxins.[9] As a result, contact-dependent mechanisms can precisely target neighboring competitors without the risk of toxin dilution in the surrounding liquid environment.[10]

The type VI secretion system (T6SS) is a widespread molecular apparatus that relies on direct contact to inject toxic effector proteins into target cells.[11] It is estimated to be found in more than 25% of gram-negative bacteria, encompassing both environmental and pathogenic species.[12] The delivery of T6SS toxins has been shown to influence microbial population compositions.[13–15] Importantly, the spatial arrangement of competing cells also impacts the T6SS and vice versa.[13,16]

The T6SS doesn't discriminate when targeting cells, owing to its indiscriminate delivery method and toxins that disrupt widely conserved cellular processes.[17] To prevent self-harm and protect kin, T6SS-positive bacteria produce matching pairs of effector and immunity proteins.[18] Yet, bacteria can possess multiple T6SS gene clusters along with variable auxiliary clusters that frequently encode additional effector and immunity proteins.[19] Incompatibility in just one of these effector-immunity pairs can drive T6SS competition.[17,20] Interestingly, targeted cells can also protect themselves through immunity-independent mechanisms, such as through the production of extracellular polysaccharides and surface-attached capsules, allowing them to survive T6SS attacks.[21–23] Furthermore, bacteria have been shown to withstand T6SS challenge and respond more potently.[23–25]

Bacterial autoaggregation is a process that allows bacteria to bind to themselves, often serving as a necessary step in forming

Please cite this article in press as: Otto et al., Interactions between pili affect the outcome of bacterial competition driven by the type VI secretion system, Current Biology (2024), https://doi.org/10.1016/j.cub.2024.04.041

biofilms.[26,27] This phenomenon is frequently linked to pathogenicity as it provides protection against external threats, such as phagocytosis[28] and antimicrobial agents.[29,30] Various molecules/structures, often referred to as autoagglutinins, can facilitate this cell-to-cell binding.[31] Here, we specifically focus on type IV pili (T4Ps), which are common surface-exposed appendages with diverse functions, including DNA uptake, motility, adhesion, and aggregation.[32,33] T4P's ability to sense the environment is crucial for the survival, colonization, and virulence of species carrying these pili.[34] For instance, the toxin co-regulated pilus, exclusive to the pandemic lineage of *Vibrio cholerae*, plays a critical role in host and interbacterial cell adhesion, which is vital for pathogenesis.[35] Similarly, T4Ps mediate interbacterial interactions in other pathogens like *Pseudomonas aeruginosa* and *Neisseria meningitidis*.[36,37] However, this ability to sense the environment and interact with other bacteria might inadvertently lead to unwanted cell-to-cell contact, potentially inviting competition from the T6SS. It is therefore worth noting that many autoagglutinins, including T4Ps, can modulate their level of aggregation.[31,38]

To explore the impact of the T6SS on bacterial behavior in the context of T4P-mediated cell-to-cell contact, we selected *V. cholerae* as our model organism. This bacterium is notable for possessing both a T6SS and a variable DNA-uptake T4P. Indeed, in *V. cholerae* strains, a single T6SS machinery is responsible for delivering distinct antibacterial effectors. These effectors are encoded within three genetic clusters, including the primary large gene cluster that houses most of the structural components, as well as auxiliary clusters 1 and 2.[19] In some *V. cholerae* strains, including the current pandemic lineage, there are additional auxiliary clusters that contain extra effector-immunity pairs, although their presence varies.[20,39–41] It is worth noting that in the aquatic environment, the presence of chitin degradation products has a dual effect on *V. cholerae*: it activates both the T6SS machinery and the DNA-uptake T4P as part of the bacterium's natural competence program. Consequently, T6SS-mediated neighbor predation leads to DNA acquisition, ultimately driving horizontal gene transfer through the process of natural transformation.[42–44] In the current pandemic strains of *V. cholerae*, this activation is orchestrated by the TfoX master regulator once the bacteria reach a high cell density state.[42,43,45,46] In environmental *V. cholerae* isolates, the T6SS machinery is in a state of constant activity,[20,47–50] representing an immediate risk for T6SS-associated harm in cases where cell-to-cell contact is established. Therefore, bacteria must distinguish between nearby individuals before intentionally initiating cell-to-cell contact.

Prior research has shown that the DNA-uptake T4P, present in all *V. cholerae* strains, often self-interacts and that it can distinguish between strains based on the variability of the major pilin protein, PilA.[51] Interestingly, such variability in the major pilin protein has been observed in various species carrying T4Ps.[52–54] Our hypothesis therefore centers on the potential of T4Ps to be harnessed for targeted T6SS-mediated bacterial elimination by facilitating specific cell-to-cell contact. Notably, in spotted microcolonies of *Neisseria cinerea*, loss of T4Ps influenced prey survival,[55] highlighting the potential for T4Ps to enhance T6SS killing. In contrast, recent findings by the Filloux group revealed that in *P. aeruginosa*, T4P-mediated surface twitching motility serves as a defensive mechanism by minimizing interspecies contacts, thus enabling prey bacteria to escape T6SS attacks.[15]

Typically, studies exploring T6SS-mediated killing are conducted on agar surfaces at high cell densities, where physical contact is forced due to crowding. In contrast, T4Ps could enable cell-to-cell contact with particular target cells under non-crowded (e.g., liquid) growth conditions, an idea that we tested in this study. We also sought to investigate the relationship between the natural diversity of PilA and the T6SS, aiming to uncover the strategies bacteria might employ to regulate the risk associated with establishing cell-to-cell contact. Finally, we used simulations to determine the factors that might either enable or impede the predation of T4P-carrying bacteria. Our simulations also emphasize the critical role of spatial organization and rapid lysis in the success of T6SS-mediated targeted depletion. Collectively, our study demonstrates that the natural diversity of T4Ps plays a pivotal role in regulating the extent of non-kin cell-to-cell contact, thus shaping the ensuing competition driven by the T6SS.

RESULTS AND DISCUSSION

T4Ps facilitate T6SS-mediated killing by fostering cell-to-cell contact

We hypothesized that T4P-mediated autoaggregation might enhance the essential cell-to-cell contact necessary for T6SS-mediated elimination under liquid conditions. To test our hypothesis, we induced the activity of both T6SS and T4Ps by artificial production of the TfoX master regulator.[43] We then co-cultured T6SS-competent strains (acting as predator) with T6SS-sensitive target strains (prey). We made the prey strains T6SS-sensitive by deleting the genes encoding the four T6SS effector/immunity protein pairs (Δ4E/I), a modification applied to the pandemic *V. cholerae* strain A1552, which served as the chassis for our research throughout this study. Predator strains were engineered to be either T6SS-competent or rendered non-functional by deleting *vasK*, which encodes a critical component of the T6SS membrane complex.[56]

To investigate the role of T4Ps, we manipulated the major pilin PilA of A1552, a pivotal T4P component. We either kept the encoding gene in its original genetic location (*pilA*(A1552)) or deleted it (Δ*pilA*) in both the predator and prey strains. In all strains, we disabled T4P retraction (Δ*pilT*), which promoted an intensified autoaggregation effect.[51] The phenomenon of amplified autoaggregation due to *pilT* deletion has also been observed in other bacteria, such as *N. meningitidis*.[57] In this study, we employed *pilT* deletion as a practical approach to increase the likelihood of self-interactions between pili. However, it's worth noting that these enhanced self-interactions may resemble the interactions of T4Ps on chitin surfaces, where dense networks of pili-pili interactions are well-documented.[51] Unfortunately, performing experiments on chitin surfaces proved to be technically unfeasible for testing the hypotheses outlined above.

The ability of strains to outcompete one another was determined by the log-transformed relative competitive index (RCI), which compares the strain-1-to-strain-2 ratio at the end of the experiment with the starting one (see section bacterial competition assays in STAR Methods).[35,58] Here, positive

Please cite this article in press as: Otto et al., Interactions between pili affect the outcome of bacterial competition driven by the type VI secretion system, Current Biology (2024), https://doi.org/10.1016/j.cub.2024.04.041

CellPress
OPEN ACCESS

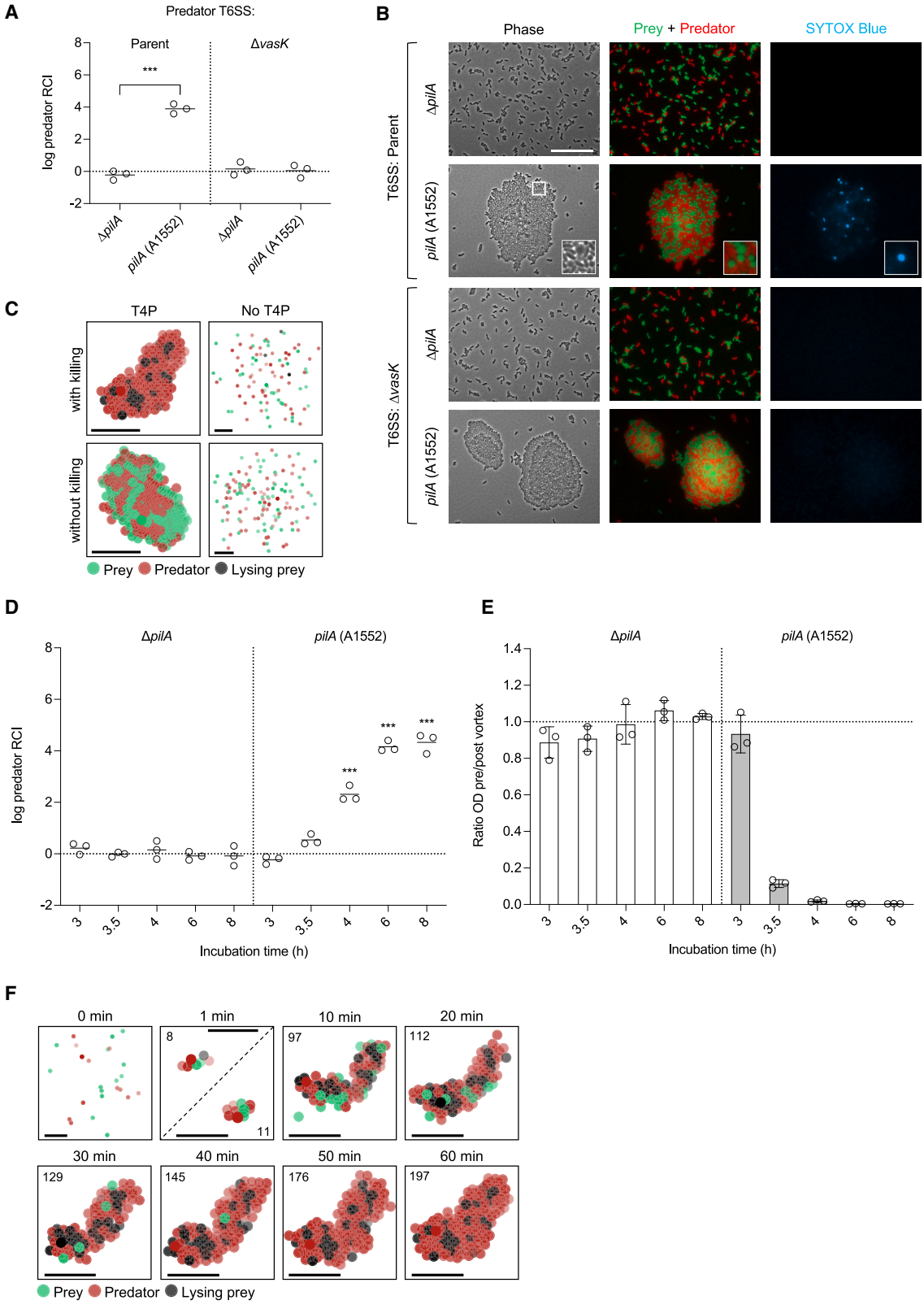

(legend on next page)

Please cite this article in press as: Otto et al., Interactions between pili affect the outcome of bacterial competition driven by the type VI secretion system, Current Biology (2024), https://doi.org/10.1016/j.cub.2024.04.041

values of log RCI indicate that strain 1 outcompetes strain 2, while a value of 0 indicates neither strain outcompetes the other strain. To distinguish predator and prey strains, we used distinct antibiotic/fluorescent markers. Notably, strains solely carrying these markers displayed no change in relative abundance when competed against a A1552Δ*lacZ* reference strain (Figure S1A; see section bacterial competition assays in STAR Methods).[35,58]

Co-culture experiments between prey and predator strains clearly demonstrated that predator strains can outcompete prey strains when the T4Ps were functionally active (Figures 1A and S1B). Conversely, when the predator strain had a non-functional T6SS, any difference in relative abundance was entirely abolished. This suggests that the change in relative abundance of predator strains is primarily achieved through T6SS-mediated depletion of prey cells.

To validate the T6SS-mediated depletion of prey cells, we conducted imaging of the co-cultures, examining the spatial arrangement of prey and predator cells (Figure 1B). In order to image aggregates, cells were grown in liquid culture, mounted on an agarose pad, covered with a coverslip, and imaged immediately (see section bacterial imaging through light microscopy in STAR Methods). In our observations, we used a cell-impermeable DNA dye (SYTOX Blue) to visualize cells with compromised membrane integrity.[59] What we witnessed was that the autoaggregation promoted by the T4Ps effectively facilitated the necessary cell-to-cell contact for T6SS-mediated cell elimination in liquid conditions. In contrast, the absence of functional T4P eliminated the cell-to-cell contact, thereby preventing the killing of T6SS-sensitive strains. Second, we noted cell rounding and lysis of T6SS-sensitive prey, a phenomenon predominantly occurring in cells in direct contact with the predator strains (Figure 1B, inset). This particular trait was dependent on the presence of a T6SS-competent predator strain, with no discernible changes in prey cell morphology when a non-functional T6SS predator strain was utilized. Thus, these images offer compelling visual evidence of T6SS-mediated prey cell elimination facilitated by the T4Ps.

To analyze the impact of the different interactions and parameters involved in the T4P-facilitated T6SS-mediated depletion of prey strains, we developed an agent-based model grounded in physical principles and incorporating key biological elements (Table 1). In this model, prey and predator bacteria were initially randomly distributed at a 1:1 ratio in a three-dimensional 40×40×40 body-centered cubic lattice modeling the liquid suspension. Subsequently, all bacteria were allowed to move diffusively within the medium, with the ability to divide and to interact through T4Ps. Predators could execute T6SS-mediated killing of neighboring prey cells, which then enter a lysing state (for further details, refer to the STAR Methods section). By enabling or disabling interactions through T4Ps and T6SS killing, we were able to qualitatively reproduce the microscopic images observed (Figure 1C). Just as in the experiments, when T4Ps were present, mixed aggregates formed, leading to the lysis of prey cells when T6SS killing was enabled. Moreover, the absence of T4Ps prevented aggregation, with T6SS killing becoming a rare event. Therefore, our minimal model serves to confirm that prey depletion is significantly enhanced when predator and prey cells adhere via T4Ps. This heightened contact between neighboring prey-predator pairs allows for more frequent T6SS killing.

In light of these observations, we were keen to delve into the dynamics of contact establishment and the subsequent elimination of prey. To investigate this, we conducted a time-course co-culture experiment in which we determined the RCI of the predator strain at different incubation times (Figure 1D). Furthermore, we assessed the levels of aggregation in these co-cultures by comparing the ratio of cells in the solution with those in the settled aggregates (Figure 1E). What we found was that the change in relative abundance of predator strains became evident when compared with a Δ*pilA* co-culture control after 3.5–4 h of incubation. This synchronization with a preceding rapid aggregation event suggests that the killing of T6SS-sensitive cells occurs

Figure 1. T4Ps facilitate T6SS-mediated killing in liquid by promoting autoaggregation

(A) Relative competitive index (RCI) of T6SS-competent (parent) and non-functional (Δ*vasK*) predator strains when co-cultured with T6SS-sensitive (Δ4E/I) prey strains. Both prey and predator strains carry their native major pilin gene (*pilA*(A1552)) or lack it (Δ*pilA*). Positive log RCI values indicate the predator strain outcompeted the prey strain, and a log RCI value of 0 indicates neither strain outcompeted the other strain. RCI values were determined after 6 h of growth.

(B) Representative microscopic images depicting 4-h-old co-cultures of T6SS-competent (parent) and non-functional (Δ*vasK*) predator strains, alongside T6SS-sensitive (Δ4E/I) prey strains. Both prey and predator strains either possess their native major pilin gene (*pilA*(A1552)) or lack it (Δ*pilA*). The images include phase contrast (left), a merged view of prey (superfolder GFP [sfGFP], in green) and predator strains (mCherry, in red) (middle), and SYTOX blue dead cell stain (in blue) (right). An inset provides a zoomed-in view of an aggregate indicated on the phase channel image by a white box. Scale bars, 25 μm.

(C) Zoomed snapshots taken after 1 h from the start of the simulations, conducted as described in the STAR Methods section computational model development and testing. Of note, simulations were conducted from the 3-h mark in the experiments. The simulations consider T4P self-interactions (left vs. right column) and T6SS-mediated killing (top vs. bottom row) either enabled or disabled.

(D) Time-course analysis of log RCI of predator strains in co-culture experiments, comparing *pilA*-carrying co-cultures with corresponding *pilA*-deleted co-cultures.

(E) Time-course of co-culture experiments demonstrating the aggregation level at indicated incubation times followed by a settling time of 5 min. The aggregation level is determined by the ratio of the co-culture's optical density at 600 nm (OD_{600}) pre/post-vortex. The horizontal dotted line represents the value around which no aggregation occurs.

(F) Evolution over time of a simulated aggregate with matching T4Ps and T6SS killing. Within each panel, the number of bacteria forming the displayed aggregate is indicated. In the second panel (1 min), we show two randomly chosen small aggregates (the dashed line separating the two plots indicates that they are not close to each other), but note that other aggregates or isolated bacteria later end up within the displayed aggregate. In (A), (D), and (E), graphs show the mean, with error bars giving the standard deviation; circles represent data from three independent experiments. In dot plots, significant differences were determined using one-way ANOVA with Tukey's post hoc test (***$p < 0.001$), and p values are provided in the source data file. In (C) and (F) from simulations, prey and predator cells are represented by green and red markers, respectively, while lysing cells are indicated by black markers. The black scale bar indicates the length of 5 marker diameters. In the "no T4P" and "0 min" panels, we display the content of an arbitrary cube, of edge about 23 cell diameters, extracted from the system. See STAR Methods section computational model development and testing for further details on simulations. See also Figures S1 and S5 and Videos S1, S2, S3, and S4.

Please cite this article in press as: Otto et al., Interactions between pili affect the outcome of bacterial competition driven by the type VI secretion system, Current Biology (2024), https://doi.org/10.1016/j.cub.2024.04.041

Table 1. Model parameters

Parameter	Value	Source
Division rate k_{div}	1.58 h^{-1}	see STAR Methods section division
Killing rate k_{kill}	6.25[a]–31.25 h^{-1}	k_{fire} from Smith et al.,[64,65] and $k_{kill} = k_{fire}/z$, where z is the number of neighbors per site in the lattice
Lysis rate k_{lysis}	0.8[a]–8 h^{-1}	Smith et al.[64,65]
Diffusion coefficient D	3×10^{-12}[a]–10^{-9} $m^2.s^{-1}$	see STAR Methods section transport
Interaction energies E_{prey}, $E_{predator}$, E_{cross}	0 – 4 kT	see STAR Methods section interactions via T4P

See also Figure S5 and STAR Methods.
[a]Default values.

shortly after cell-to-cell contact is established. Similar to the experimental observations, simulations exhibit rapid aggregation, followed by T6SS killing (Figure 1F; Videos S1, S2, S3, and S4). Collectively, our data demonstrate that T4P-mediated aggregation generates enough cell-to-cell contact to facilitate effective T6SS killing, even under conditions where cells are otherwise well-mixed.

Related to this role of T4Ps in facilitating T6SS-mediated killing in liquid environments, studies have demonstrated that engineered receptor-ligand interactions can lead to the targeted depletion of prey cells within bacterial communities.[60] Similarly, in *Vibrio fischeri*, a putative lipoprotein has been implicated in mediating targeted cell-to-cell contact for T6SS competition in high-viscosity liquid media.[10] It's worth noting that this lipoprotein's distribution is limited to bacterial species associated with a marine host and has no homolog in *V. cholerae*. The specificity of target recognition in this case is achieved through an unknown ligand. In various scenarios, not limited to liquid conditions, such as within microcolonies of *N. cinerea*, the expression of T4Ps by both predator and prey strains heightened the prey's vulnerability to T6SS attacks in contrast to a non-piliated control. This effect was achieved by preventing the segregation of prey from a T6SS-armed attacker.[55] These findings underscore the potential risk involved in utilizing T4Ps in the natural environment, as they can serve as potential enhancer of T6SS-mediated competition.

Naturally occurring diversity of T6SS E/I pairs and T4P pilin alleles

Having demonstrated the potential of T4Ps to facilitate T6SS-mediated killing in liquid environments, our next objective was to investigate the interplay between the naturally occurring diversity of T6SS and T4Ps in *V. cholerae*. First, we aimed to understand whether strains carrying diverse PilA variants could engage in T6SS-dependent competition. Second, we investigated whether there is co-occurrence between the *pilA* alleles and T6SS compatibility, or if other selective forces influenced the diversity of these two systems. To address these questions, we initially constructed a cladogram involving 39 *V. cholerae* genomes, comprising both environmental and patient isolates. We used *Vibrio mimicus* as an outgroup for this analysis (Figure 2A). To evaluate the diversity of the T6SS, we aligned the nucleotide sequences of the six known T6SS clusters. We then extracted the amino acid sequences of the cognate immunity proteins in the E/I protein pairs. The resulting heatmaps, displaying the percentage identity of T6SS (Figure S2), were used to group T6SS E/I modules into families (sharing over 30% identity) and subfamilies (identical sequences) consistent with methods previously developed.[17,61] This typing approach enabled us to identify six novel T6SS E/I families that could not be grouped into existing families within the large gene cluster. Additionally, it expanded our understanding of strains carrying the recently discovered auxiliary clusters 4 and 5[20,40,41] (Figure 2A).

The categorization of strains into T6SS families, as depicted to the right of the cladogram in Figure 2A, allowed us to visualize whether they are capable of coexisting, that is sharing identical T6SS modules, or if they can engage in T6SS-dependent competition. Variety in T6SS families within *V. cholerae* isolates was large, with few T6SS-compatible strains. Indeed, previous experimental data among a subset of strains showed limited compatibility between T6SS systems with diverse E/I modules.[20] Also indicated is the previously confirmed self-interaction ability of PilA, which is presented alongside the T6SS E/I modules.[51] Next, we extracted nucleotide and protein sequences based on genome annotations to construct a heatmap and a PilA cladogram (Figures 2B and S3). Notably, the studied PilA variants exhibit high variability and cluster into numerous phylogenetic groups.

Our analysis did not reveal distinct clades for either the T6SS E/I modules or PilA variants (Figures 2A and 2B). While closely related strains occasionally shared similar T6SS E/I modules and PilA variants (for example, strains 2012Env-9 and Env-390), more often, we observed diversity in both the T6SS E/I modules and PilA variants (such as SP7G and DL4215). Moreover, we did not identify evidence for co-occurrence between PilA variants and T6SS compatibility. Nonetheless, we did observe different topologies between genome-based and *pilA* trees (Figure 2B) and an average of approximately 9% lower guanine-cytosine (GC) content for both the T6SS E/I modules and *pilA*. These observations suggest that both *pilA* and T6SS E/I modules can be horizontally acquired, as previously suggested for the latter.[17,62] Notably, horizontal exchange of *pilA* alleles or T6SS E/I modules could thereby alter bacterial competition. How the exchange of *pilA* alleles would influence T6SS competition is outlined below.

T4P-facilitated neighbor predation is conserved among self-interacting PilA variants

Subsequently, we assessed whether the capacity of T4Ps to facilitate T6SS-mediated killing is conserved among different PilA variants. To investigate PilA variability, we replaced the native *pilA* locus of strain A1552 with *pilA* alleles extracted

Please cite this article in press as: Otto et al., Interactions between pili affect the outcome of bacterial competition driven by the type VI secretion system, Current Biology (2024), https://doi.org/10.1016/j.cub.2024.04.041

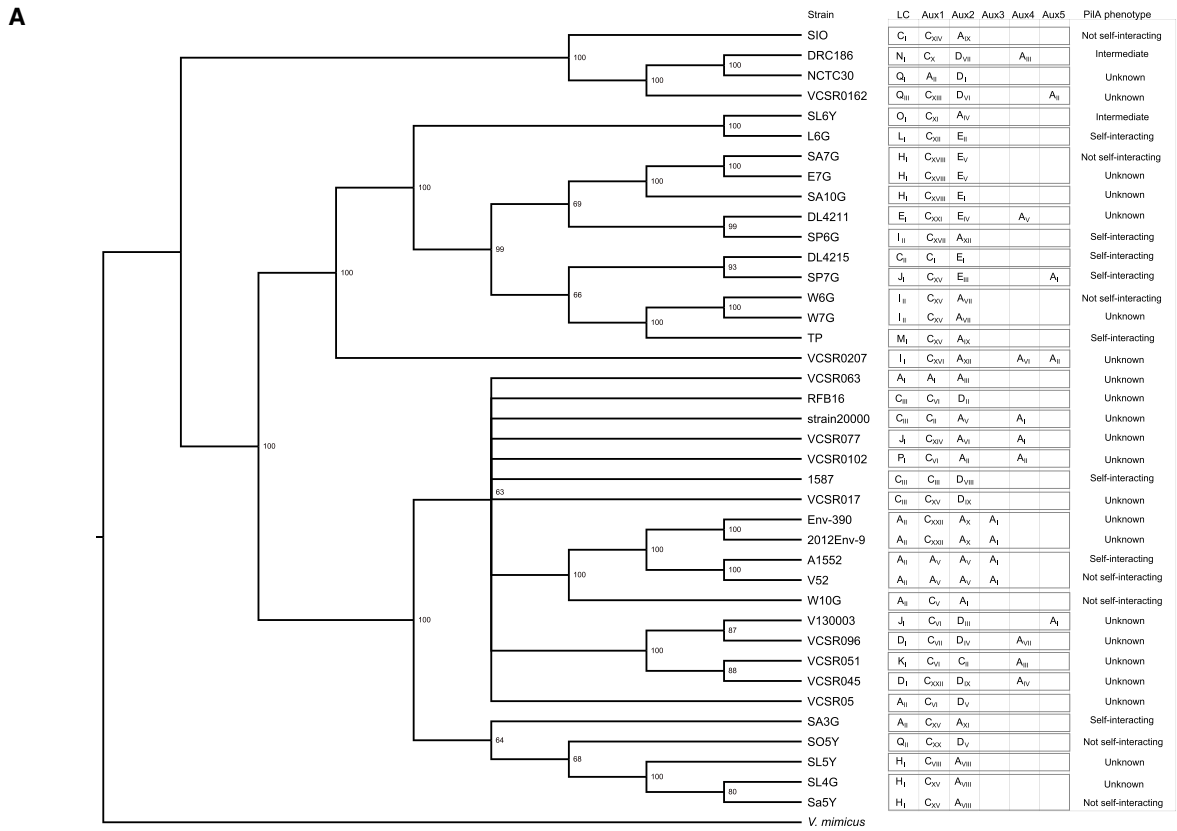

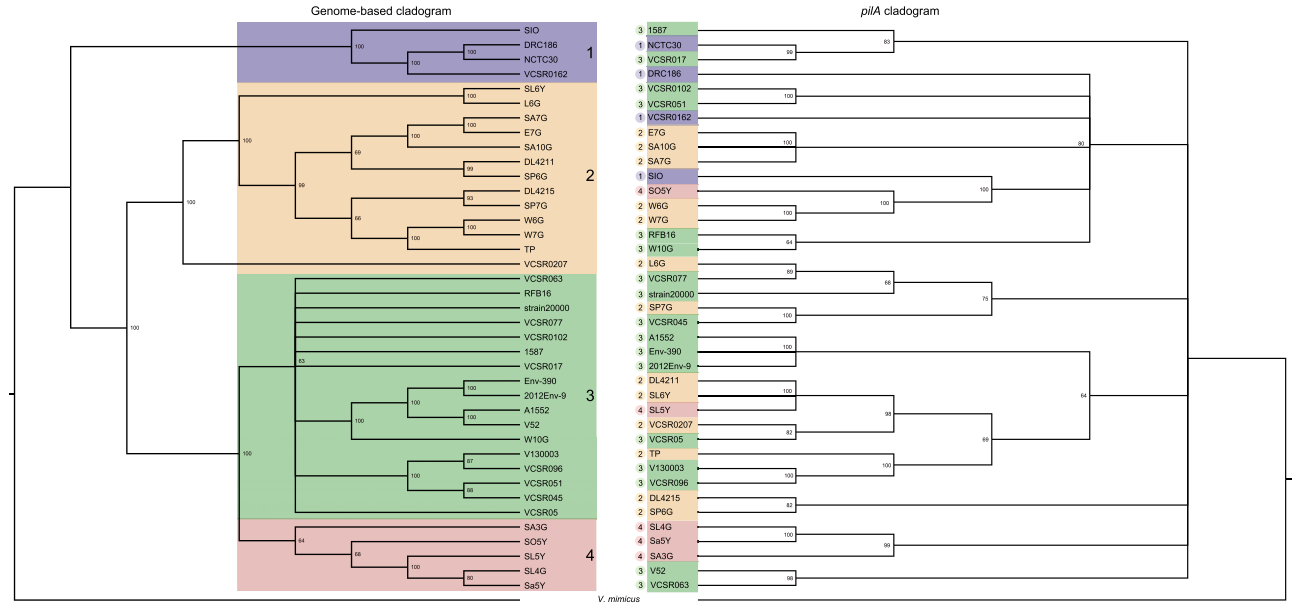

Figure 2. Diversity of T6SS E/I pairs and T4P pilin alleles in *V. cholerae*

(A) Cladogram presenting 39 *V. cholerae* strains analyzed based on 1,186 core genes. T6SS effector module families in the large (LC) and auxiliary clusters (Aux 1–5) are specified behind the strain names, followed by the self-interaction ability of T4Ps. Boxes indicate strains with identical T6SS E/I modules. *V. mimicus* (ATCC 33655) was used as an outgroup.

(legend continued on next page)

from genomes of a variety of *V. cholerae* strains, a method previously demonstrated to be fully functional.[51] The predator and prey strains with replaced *pilA* (*pilA*rep) were co-cultured, and their predator RCI was evaluated (Figures 3A and 3B). Our results revealed a positive predator RCI for PilA variants capable of self-interaction, as compared with a negative control lacking *pilA* (Δ*pilA*; Figure 3A). Conversely, PilA variants that could not self-interact according to previous work[51] were unable to facilitate T6SS-mediated killing (Figure 3B).

Interestingly, two PilA variants, from strains SL6Y and DRC186, displayed an intermediate level of prey strain depletion. Both of these PilA variants could support the killing of T6SS-sensitive prey, but the culture tubes appeared more turbid than those with other self-interacting PilA variants that mostly settled to the bottom of the tube. We hypothesized that a weaker aggregation phenotype might allow a subpopulation of targeted prey cells to escape. To explore this, we determined the aggregation levels of these PilA variants and compared them with the strongly self-interacting A1552 PilA variant and the negative Δ*pilA* control (Figure 3C). While measuring aggregation ratios,[51] various settling times were considered to allow for self-interaction of potentially weaker PilA variants. Indeed, both the SL6Y and DRC186 PilA variants exhibited weaker levels of aggregation than the strongly self-interacting A1552 PilA variant. Of these two, the SL6Y variant displayed stronger aggregation during extended settling periods, which are, however, not included in the evaluation of the predator RCI during co-culture. Notably, the major pilin of T4Ps is known to exhibit variation also in other bacterial species.[52–54] This variability can influence the strength of attractive forces between bacterial cells, as experimentally demonstrated for *Neisseria gonorrhoeae*,[63] which can explain our results. Similarly, the diversity in PilA variants in *Acinetobacter baumannii* was shown to impact the level of T4P self-interaction and its functional specialization.[54]

Pilus-specific T6SS competition by spatial segregation

A significant diversity of PilA variants is naturally present within the non-pandemic *V. cholerae* isolates.[53] We speculated that PilA diversity might provide protection for cells against T6SS competition by enabling specificity in contact establishment. To investigate this, we conducted a co-culture experiment in which we co-cultivated a prey strain with various PilA variants alongside a predator strain containing the pandemic A1552 PilA variant (Figure 4A). As expected, the presence of PilA diversity negated the ability of the predator strain to outcompete the prey strain, in contrast to the co-culture with a control T4P matching the A1552 PilA variant.

After this discovery, we proceeded to visualize the spatial arrangement of the cells, both with and without PilA diversity (Figure 4B). Although identical T4Ps led to a well-blended community with numerous interfaces of cell-to-cell contact between the two cell types, T4P diversity facilitated the predominant spatial separation of the two cell types. Consequently, due to the T4P specificity between the pandemic and other self-interacting PilA variants, T4P-mediated T6SS competition with strains carrying diverse *pilA* alleles was circumvented. We therefore conducted simulations that accounted for the presence of non-matching T4Ps incapable of cross-interaction, in contrast to matching T4Ps (Figure 4C; Videos S4 and S5). Similar to the experimental observations, prey and predator cells with diverse T4Ps formed distinct aggregates. This prevented encounters between the prey and predator, along with subsequent T6SS-mediated killings, within the timescale considered.

Most PilA variants of *V. cholerae* appear to exhibit highly specific interactions.[51] Interestingly, naturally occurring PilA variants with cross-interaction have also been identified. These promiscuous PilA variants could facilitate cell-to-cell contact between potential T6SS competitors and invite T6SS competition. We hypothesized that the potential risk of engaging in T6SS competition could be offset by preferential binding to kin. To further investigate this, we simulated prey and predator systems, in which we reduced the cross-interaction T4P binding energy (E_{cross}) between prey and predator, making cross-interaction weaker than self-interaction (Figure 4D; Video S6). These simulations resulted in patchy aggregates. Increasing E_{cross} within this range led to increased mixing within aggregates, providing more boundary interfaces between prey and predator, until the cross-interaction T4P binding energy equaled the self-interaction T4P binding energy between two prey cells or two predators, resulting in matching T4Ps. Simulating preferential binding to kin-restricted T6SS killing predominantly to the boundary interfaces between patches, thanks to the partial segregation effect arising from weaker interactions across T4P variants.

Next, we determined the spatial organization of the cells for all promiscuous interactions (Figures 4E and S4). Simultaneously, we performed co-culture experiments to evaluate the predator RCI of all known promiscuous interactions, as well as their conforming counterparts (Figure 4F). Compared with the matching A1552 PilA variant condition, we observed two distinct phenotypes. The promiscuity between SA3G and SP6G PilA variants resulted in low-level mixing, with sparse non-kin cell-to-cell contact at boundary interfaces. This led to no change in relative abundance for T6SS-competent cells at the population level, as evident from the determined predator RCI. For the other promiscuous PilA variant combinations, we observed an intermediate phenotype. Segregated groups of cell types were observed, leading to a subpopulation of cells engaging in non-kin cell-to-cell contact, while others established cell-to-cell contact between kin cells. This matches the predictions from our model, since the simulations that modeled preferential binding to kin produced aggregates of similar morphology to both types of promiscuous T4Ps (Figure 4D), depending on the exact value of the cross-interaction T4P binding energy (E_{cross}). This shows that weaker interactions between promiscuous T4P variants are responsible for the observed spatial organization patterns. The resulting patchiness leads to a reduction of T6SS competition interfaces compared with the case with matching pili and restricts the risk of T6SS competition to a subset of the population,

(B) Comparison of the core gene-based cladogram of the 39 *V. cholerae* strains studied (on the left side) with the *pilA* nucleotide-sequence-based cladogram (on the right side). Colored boxes highlight supported clades of relatively related strains, which are also represented by colored circles in the *pilA* cladogram. The difference in topologies between the genome-based and *pilA* reconstructions suggests horizontal movement of the *pilA* genes. Statistical significance was verified using 100 bootstraps, and nodes with bootstrap values below 60 were collapsed. See also Figures S2 and S3.

Please cite this article in press as: Otto et al., Interactions between pili affect the outcome of bacterial competition driven by the type VI secretion system, Current Biology (2024), https://doi.org/10.1016/j.cub.2024.04.041

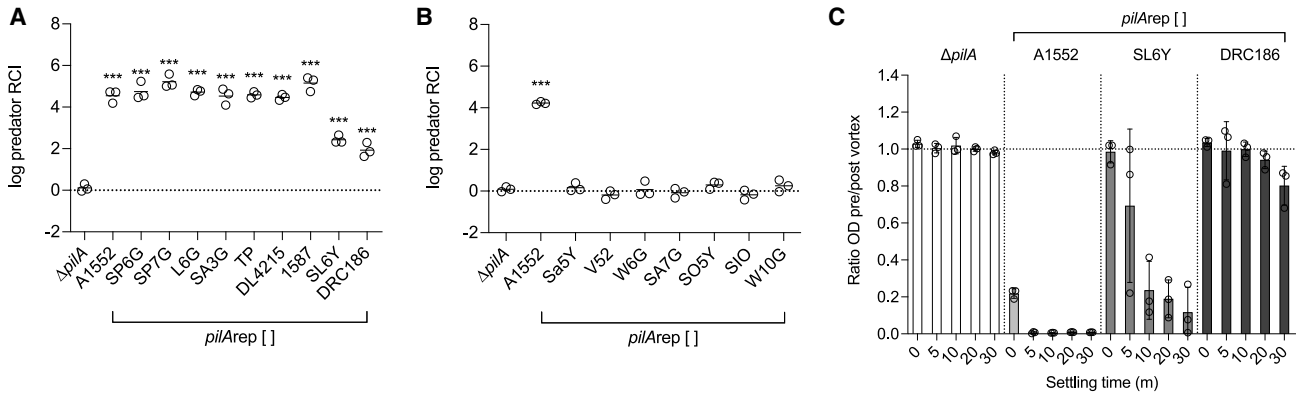

Figure 3. Conservation of T4P-mediated T6SS killing across self-interacting PilA variants

(A) Bacterial competition assay introducing self-interacting PilA variants into T6SS-competent (predator) and T6SS-sensitive (prey) strains.

(B) Log RCI of non-interacting PilA variants, with self-interacting *pilA*rep[A1552] serving as a positive control.

(C) Aggregation assay assessing the aggregation level of PilA variants from strains SL6Y and DRC186 compared with the one from A1552. Cultures are allowed to settle for the specified duration, after which the aggregation level was determined by calculating the ratio of the culture's OD_{600} before and after vortexing. The horizontal dotted line denotes the ratio around which no aggregation occurs. The Δ*pilA* strain serves as the negative control. Circles in graphs represent independent replicates, while bars/lines indicate the mean, with error bars illustrating the standard deviation. Log-transformed RCI values of predators were compared with Δ*pilA* for statistical analysis (ANOVA with Tukey's post hoc test; $^{***}p < 0.001$), and *p* values are provided in the source data file.

resembling a bet-hedging strategy. Alternatively, intrinsically modulating the strength or ability of T4Ps to self-interact (e.g., SL6Y/Sa5Y) would reduce the number of all T4P-facilitated cell-to-cell contacts but may affect the functional specialization of the strain. Lastly, the predominant PilA variant specificity found in naturally occurring isolates suggests a selective burden for non-specific T4Ps. Although we demonstrate that T6SS competition could apply a selective burden for pilus conformity, we suggest that diversity in both T6SS and PilA is also driven by factors independent of their interplay. Namely, T4P-independent T6SS competition, potentially caused through proximity by crowding, could also drive the diversity observed in T6SS E/I modules, while the PilA variability might reflect the selection pressure by other stressors, such as phage predation.

Spatial assortment and lysis time dictate T6SS-mediated target cell depletion

With evidence of the T4P's potential in facilitating T6SS depletion, we aimed to explore the key factors influencing its effectiveness using our agent-based model. Considering the observed ability of T4Ps to regulate non-kin cell-to-cell contact, we assessed the impact of cross-interaction T4P binding energy on mixing levels (Figure 5A). To analyze the mixing within aggregates in more detail, we evaluated assortment, which compares the number of observed adjacent prey-predator pairs with its maximum expected value, which is obtained in the case of random mixing (see section assortment: characterization of mixing within aggregates in STAR Methods). Similar to the experimental observations, our simulations demonstrate that a non-zero cross-interaction T4P binding energy (E_{cross}) between prey and predator increases assortment, thereby promoting mixing. Higher cross-interaction T4P binding energy between prey and predator results in the formation of more mixed aggregates, with larger E_{cross} values leading to increased spatial assortment. Moreover, we noted a stronger, long-term, gradual rise in assortment over time in the presence of T6SS killing compared with scenarios without T6SS killing. The action of T6SS results in a decrease of the number of prey cells, making the remaining ones isolated and surrounded by predators, which increases assortment. Our main observations about assortment are robust to changes of the killing and lysis rates within the physiological range (Figure S5A). After infinite time, all T6SS killing simulations would eventually become uniform, consisting solely of predators, corresponding to the fixation of the predator type. However, it is crucial to highlight that our simulations do not account for the potential escape of prey cells into new niches. In natural settings, the observed delay in spatial assortment for lower values of E_{cross} could potentially be exploited by the T6SS-sensitive prey.

Having shown how T4P cross-interactions shape spatial assortment, we aimed to determine the impact of these interactions on the predator RCI (Figure 5B). We observed a rapid increase in the log RCI with time, greatly influenced by the value of the prey-predator T4P binding energy. When $E_{cross} = 0$, this increase was minimal within the timescale considered. Therefore, strong T4P-mediated attraction between prey and predator plays a crucial role in promoting T6SS competition, a condition achieved by matching T4Ps and modulated by promiscuous T4Ps. We observe that assortment (Figure 5A) and log RCI (Figure 5B) have similar overall time evolutions here. These two quantities are truly different in principle since assortment characterizes local mixing while RCI is a global quantity that gives insight into the overall composition of the system. However, here, no mixing (assortment close to zero) entails no killing (log RCI close to zero) because prey-predator contacts are needed for killing. Hence, the similar time evolution of assortment and of log RCI is due to the fact that T4Ps mediate killing by T6SS. We observed a positive relationship between the predator RCI and E_{cross}, with T6SS competition being enhanced as prey-predator attraction increases toward a matching T4P condition (Figure 5C). Matching T4Ps ensure a strong binding energy between cell types, leading to the subsequent T6SS depletion of target strains, while diverse T4Ps hinder T6SS competition, depending

Please cite this article in press as: Otto et al., Interactions between pili affect the outcome of bacterial competition driven by the type VI secretion system, Current Biology (2024), https://doi.org/10.1016/j.cub.2024.04.041

CellPress
OPEN ACCESS

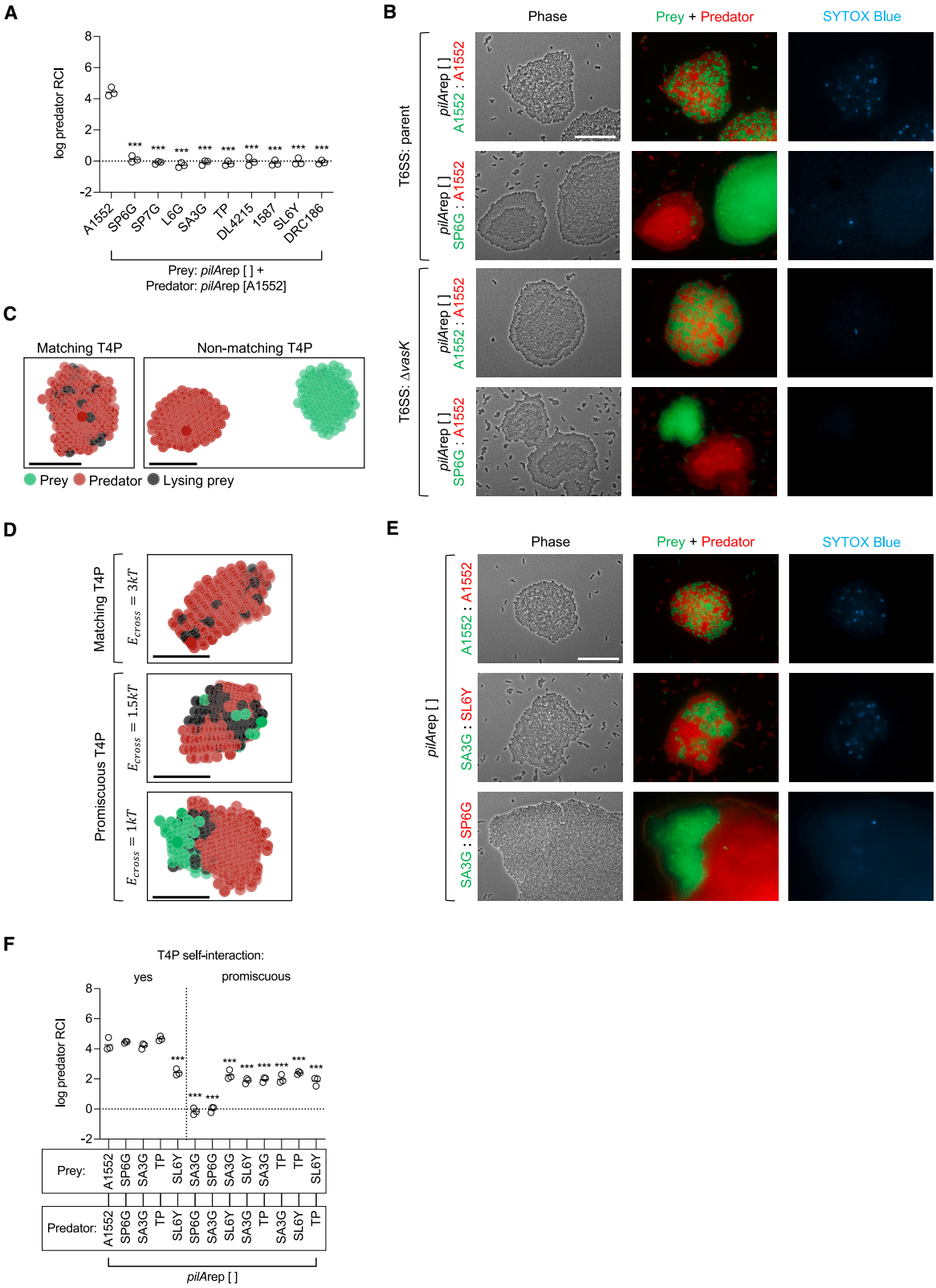

Figure 4. Impact of pilus specificity on T6SS competition and spatial segregation

(A) Log RCI of T6SS-competent (predator) strains competing with T6SS-sensitive (prey) strains, with diverse PilA variants among the prey strains, against a predator strain carrying the A1552 PilA variant. Details as described for Figure 3.

(legend continued on next page)

Please cite this article in press as: Otto et al., Interactions between pili affect the outcome of bacterial competition driven by the type VI secretion system, Current Biology (2024), https://doi.org/10.1016/j.cub.2024.04.041

on the level of promiscuity of the PilA variant. Through PilA diversity, spatial assortment is modulated, dictating the dynamics of T6SS-mediated depletion of target strains by altering the level of T6SS competition interfaces. Indeed, autoaggregation facilitated by self-interacting identical T4Ps could function as a defense strategy of *V. cholerae* against T6SS invaders.

Interestingly, the reduction in T6SS competition interfaces observed in the simulations and imaging of promiscuous T4Ps resulted in lysing cells forming a barrier between cell types. This phenomenon, known as the corpse barrier effect,[64] could significantly influence the dynamics of prey depletion. To further investigate this, we determined the log predator RCI for various lysis times (Figure 5D).[65] We observed a negative relationship between lysis time and log predator RCI. Consistent with the findings of Smith and colleagues,[64] the corpse barrier effect impedes T6SS competition by obstructing predators from reaching new targets. Predator cells equipped with fast-acting lysing effector modules could overcome this barrier, which might be a critical factor in considering target depletion. In *V. cholerae*, strain W10G, carrying two pandemic-like A-type E/I modules in the large and aux2 clusters, has been shown to exhibit strong killing activity against other environmental *V. cholerae* strains.[20] Moreover, *Vibrio coralliilyticus*, while not resistant to *V. cholerae* T6SS attacks, can withstand T6SS challenge and deplete a non-pandemic O1 serogoup *V. cholerae* strain through T6SS killing.[25] These are examples of potent T6SS strains/species, though whether this is due to rapid lysis, or other factors, e.g., firing rate, remains to be determined. Lastly, spatial assortment could prevent the formation of a corpse barrier, as demonstrated in our experiments. Mixing between predator and prey cells, promoted by matching T4Ps, increases T6SS competition interfaces. However, it remains to be investigated whether this mixing occurs under natural conditions.

Notably, in this study, we artificially induce T4Ps and T6SS and use retraction-deficient cells as a powerful tool to study their interplay. Thus, an important question for future research will be to comprehend whether under natural conditions, e.g., chitin surfaces for *V. cholerae*, T4Ps could serve as a means for the recruitment of predator cells. This exploration could also yield further insights into the consequences of T6SS and T4Ps on the local enrichment of pathogenic or environmental strains, as well as PilA variant specialization for *V. cholerae*, specifically. Nonetheless, the swift capture and subsequent elimination of pandemic *V. cholerae* through pilus conformity observed in our experiments have demonstrated the potential for the targeted depletion of T4P-carrying species.

The critical role of self-interacting T4Ps in the colonization of pathogen hosts and environmental niches may contribute to the maintenance of the targeted receptor. For instance, in *V. cholerae*, the conservation of the strongly self-interacting PilA variant within the pandemic lineage suggests its significance in the aquatic environment and/or during human transmission.[51] Additionally, the preservation of T4P specificity might prevent T4P-facilitated competition with T6SS-carrying competitors. In contrast, the self-interacting toxin co-regulated pilus, exclusive to the *V. cholerae* pandemic lineage, does not display target specificity between major pilin variants.[51,66] It is important to note that the T6SS E/I modules of pandemic strains are identical, rendering them T6SS compatible. Finally, considering the natural occurrence of diverse self-interacting T4Ps in various pathogens,[31,52–54] the investigation of targeted depletion using T4Ps should be pursued further.

STAR★METHODS

Detailed methods are provided in the online version of this paper and include the following:

- KEY RESOURCES TABLE
- RESOURCE AVAILABILTY
  - Lead contact
  - Materials availability
  - Data and code availability
- EXPERIMENTAL MODEL AND SUBJECT DETAILS
  - Bacterial strains
  - Growth conditions
- METHOD DETAILS
  - Bacterial strain engineering
  - Bacterial competition assays
  - Bacterial imaging through light microscopy
  - Bacterial aggregation assay
  - Computational model development and testing
  - Bioinformatical analysis and phylogeny
- QUANTIFICATION AND STATISTICAL ANALYSIS

SUPPLEMENTAL INFORMATION

Supplemental information can be found online at https://doi.org/10.1016/j.cub.2024.04.041.

ACKNOWLEDGMENTS

We thank Milena Jaskólska for provision of the codon-optimized mCherry construct, Milena Jaskólska and David W. Adams for their contribution to the mentoring of S.B.O., and members of the Blokesch and Bitbol laboratories for fruitful discussions. This work was supported by grants from the Swiss

(B) Representative microscopy images of co-culture experiments between T6SS-competent (parent) or non-functional (Δ*vasK*) predator strains, and T6SS-sensitive (Δ4E/I) prey strains. Predator and prey strains are either carrying matching (A1552: A1552) or diverse (SP6G: A1552) PilA variants. Details as described for Figure 1B.

(C) Snapshots from simulations after 1 h (corresponding to the 4-h mark in experiments), with different T4P-mediated binding energy (E_{cross}) between predators and prey. E_{cross} was set at 3 kT for matching T4Ps and 0 for diverse T4Ps. Details as described for Figures 1C and 1F.

(D) Snapshots from simulations after 1 h, representing various levels of T4P promiscuity obtained by modulating the T4P-mediated binding energy E_{cross}, compared with a matching T4P control. Details as described for Figures 1C and 1F.

(E) Imaging of co-culture experiments between T6SS-competent (predator) and T6SS-sensitive (prey) strains, featuring PilA variants with varying levels of promiscuousness. Details as described for Figure 1B.

(F) Log RCI in prey/predator co-culture experiments, where the PilA variants display varying degrees of promiscuous T4P-mediated self-interactions. Circles in graphs represent independent experiments, and means are indicated by lines. Statistical tests were compared with the (non-promiscuous) matching *pilA*rep [A1552] control condition using one-way ANOVA with Tukey's post hoc test (***$p < 0.001$), and p values are provided in the source data file. See also Figures S4 and S5 and Videos S1, S4, S5, and S6.

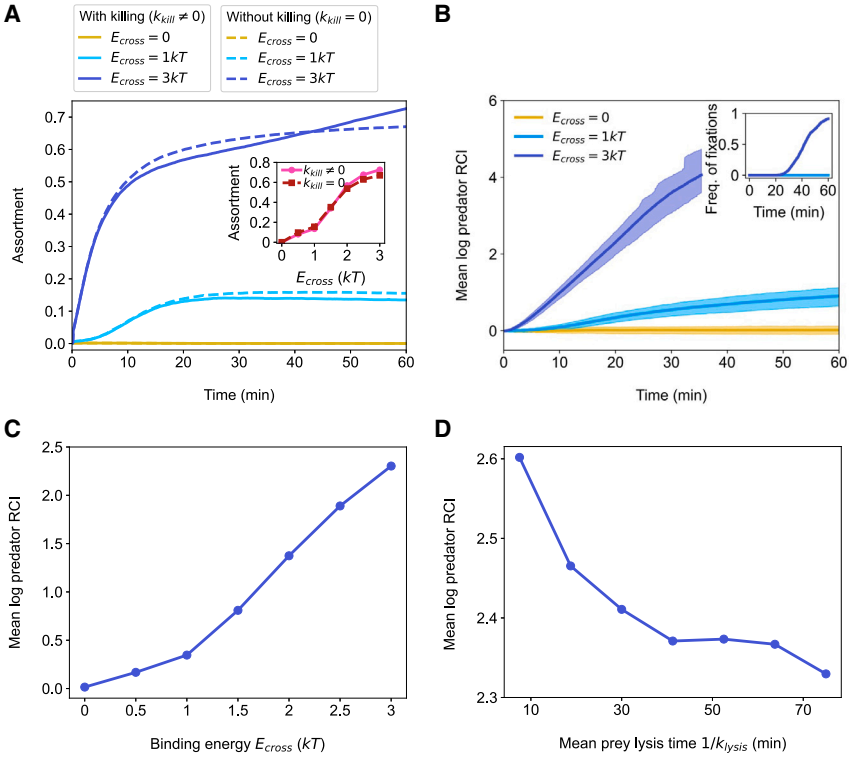

Figure 5. Impact of T4P-mediated binding energy and lysis time on spatial assortment and log predator RCI

(A) Impact of the attractive interaction between prey and predators on mixing over time. The main panel displays the assortment between prey and predators over time, averaged over simulation replicates, for different values of the T4P binding energy E_{cross} between a prey and a predator. Solid lines represent simulations with killing ($k_{kill} = 6.25\ h^{-1}$), while dashed lines depict scenarios without killing ($k_{kill} = 0$). Assortment is determined by comparing the number of adjacent prey-predator pairs with its maximum expected value, considering lysing cells as prey (see STAR Methods section assortment: characterization of mixing within aggregates). The inset graph shows assortment vs. E_{cross} after 1 h of simulations (corresponding to the 4-h mark in experiments).

(B) Evolution of RCI over time. The main panel depicts the mean log RCI vs. time for various E_{cross} values. The inset shows the frequency of fixation events, where only predators remain, and prey are completely depleted, across the replicate simulations. When fixation occurs in a replicate, the RCI diverges and is thus excluded from the calculation of the mean RCI. To address potential bias, the results are only displayed until the frequency of fixations reaches 0.25 for $E_{cross} = 3$ kT. The shaded areas represent the interquartile ranges.

(C) Impact of attraction between prey and predators on the resulting predator RCI. The graph displays the mean log RCI vs. E_{cross} after 20 min of simulation.

(D) Effect of lysis time on prey depletion. The mean log RCI is shown vs. the mean lysis time ($1/k_{lysis}$) after 20 min of simulation with $E_{cross} = 3$ kT. When fixation occurs in a replicate simulation, the corresponding RCI diverges and is therefore not considered in the calculation of the mean RCI. Fixation events were observed in less than 0.5% of replicate simulations. All results are averaged over 10^3 replicate simulations. See also Figure S5.

National Science Foundation (310030_185022) and the European Research Council (grant agreement no. 724630) and an International Research Scholarship by the Howard Hughes Medical Institute (55008726) awarded to M.B. R.S. and A.-F.B. acknowledge funding from the European Research Council (ERC) under the European Union's Horizon 2020 research and innovation programme (grant agreement no. 851173, to A.-F.B.).

AUTHOR CONTRIBUTIONS

S.B.O. and M.B. conceived the project and designed and analyzed the biological experiments. S.B.O. constructed strains and plasmids and performed all biological experiments. R.S. and A.-F.B. designed and analyzed the computational model and the numerical simulations. R.S. performed all numerical simulations. A.L. performed bioinformatic analyses. S.B.O. and M.B. wrote the manuscript with input from A.L., R.S., and A.-F.B. M.B. and A.-F.B. acquired funding and supervised the project.

DECLARATION OF INTERESTS

The authors declare no competing interests.

DECLARATION OF GENERATIVE AI AND AI-ASSISTED TECHNOLOGIES IN THE WRITING PROCESS

During the preparation of this work, the author(s) used ChatGPT for English editing. After using this tool/service, the author(s) reviewed and edited the content as needed and take(s) full responsibility for the content of the publication.

Received: October 26, 2023
Revised: April 9, 2024
Accepted: April 22, 2024
Published: May 14, 2024

REFERENCES

1. Shin, N.-R., Whon, T.W., and Bae, J.-W. (2015). Proteobacteria: microbial signature of dysbiosis in gut microbiota. Trends Biotechnol. *33*, 496–503. https://doi.org/10.1016/j.tibtech.2015.06.011.
2. Zheng, Q., Hu, Y., Zhang, S., Noll, L., Böckle, T., Dietrich, M., Herbold, C.W., Eichorst, S.A., Woebken, D., Richter, A., et al. (2019). Soil multifunctionality is affected by the soil environment and by microbial community composition and diversity. Soil Biol. Biochem. *136*, 107521. https://doi.org/10.1016/j.soilbio.2019.107521.
3. Foster, K.R., and Bell, T. (2012). Competition, not cooperation, dominates interactions among culturable microbial species. Curr. Biol. *22*, 1845–1850. https://doi.org/10.1016/j.cub.2012.08.005.
4. Ghoul, M., and Mitri, S. (2016). The ecology and evolution of microbial competition. Trends Microbiol. *24*, 833–845. https://doi.org/10.1016/j.tim.2016.06.011.
5. Russel, J., Røder, H.L., Madsen, J.S., Burmølle, M., and Sørensen, S.J. (2017). Antagonism correlates with metabolic similarity in diverse bacteria. Proc. Natl. Acad. Sci. USA *114*, 10684–10688. https://doi.org/10.1073/pnas.1706016114.
6. Smith, W.P.J., Wucher, B.R., Nadell, C.D., and Foster, K.R. (2023). Bacterial defences: mechanisms, evolution and antimicrobial resistance. Nat. Rev. Microbiol. *21*, 519–534. https://doi.org/10.1038/s41579-023-00877-3.
7. García-Bayona, L., and Comstock, L.E. (2018). Bacterial antagonism in host-associated microbial communities. Science *361*, eaat2456. https://doi.org/10.1126/science.aat2456.
8. Klein, T.A., Ahmad, S., and Whitney, J.C. (2020). Contact-dependent interbacterial antagonism mediated by protein secretion machines. Trends Microbiol. *28*, 387–400. https://doi.org/10.1016/j.tim.2020.01.003.

9. Ikryannikova, L.N., Kurbatov, L.K., Gorokhovets, N.V., and Zamyatnin, A.A. (2020). Contact-dependent growth inhibition in bacteria: do not get too close! Int. J. Mol. Sci. *21*, 7990. https://doi.org/10.3390/ijms21217990.

10. Speare, L., Woo, M., Dunn, A.K., and Septer, A.N. (2022). A putative lipoprotein mediates cell-cell contact for Type VI secretion system-dependent killing of specific competitors. mBio *13*, e0308521. https://doi.org/10.1128/mbio.03085-21.

11. Coulthurst, S. (2019). The Type VI secretion system: a versatile bacterial weapon. Microbiology (Reading) *165*, 503–515. https://doi.org/10.1099/mic.0.000789.

12. Bingle, L.E.H., Bailey, C.M., and Pallen, M.J. (2008). Type VI secretion: a beginner's guide. Curr. Opin. Microbiol. *11*, 3–8. https://doi.org/10.1016/j.mib.2008.01.006.

13. McNally, L., Bernardy, E., Thomas, J., Kalziqi, A., Pentz, J., Brown, S.P., Hammer, B.K., Yunker, P.J., and Ratcliff, W.C. (2017). Killing by Type VI secretion drives genetic phase separation and correlates with increased cooperation. Nat. Commun. *8*, 14371. https://doi.org/10.1038/ncomms14371.

14. Robitaille, S., Simmons, E.L., Verster, A.J., McClure, E.A., Royce, D.B., Trus, E., Swartz, K., Schultz, D., Nadell, C.D., and Ross, B.D. (2023). Community composition and the environment modulate the population dynamics of type VI secretion in human gut bacteria. Nat. Ecol. Evol. *7*, 2092–2107. https://doi.org/10.1038/s41559-023-02230-6.

15. Rudzite, M., Subramoni, S., Endres, R.G., and Filloux, A. (2023). Effectiveness of *Pseudomonas aeruginosa* type VI secretion system relies on toxin potency and type IV pili-dependent interaction. PLoS Pathog. *19*, e1011428. https://doi.org/10.1371/journal.ppat.1011428.

16. Borenstein, D.B., Ringel, P., Basler, M., and Wingreen, N.S. (2015). Established microbial colonies can survive Type VI secretion assault. PLoS Comput. Biol. *11*, e1004520. https://doi.org/10.1371/journal.pcbi.1004520.

17. Unterweger, D., Miyata, S.T., Bachmann, V., Brooks, T.M., Mullins, T., Kostiuk, B., Provenzano, D., and Pukatzki, S. (2014). The *Vibrio cholerae* type VI secretion system employs diverse effector modules for intraspecific competition. Nat. Commun. *5*, 3549. https://doi.org/10.1038/ncomms4549.

18. Russell, A.B., Hood, R.D., Bui, N.K., LeRoux, M., Vollmer, W., and Mougous, J.D. (2011). Type VI secretion delivers bacteriolytic effectors to target cells. Nature *475*, 343–347. https://doi.org/10.1038/nature10244.

19. Pukatzki, S., McAuley, S.B., and Miyata, S.T. (2009). The type VI secretion system: translocation of effectors and effector-domains. Curr. Opin. Microbiol. *12*, 11–17. https://doi.org/10.1016/j.mib.2008.11.010.

20. Drebes Dörr, N.C., and Blokesch, M. (2020). Interbacterial competition and anti-predatory behaviour of environmental *Vibrio cholerae* strains. Environ. Microbiol. *22*, 4485–4504. https://doi.org/10.1111/1462-2920.15224.

21. Toska, J., Ho, B.T., and Mekalanos, J.J. (2018). Exopolysaccharide protects *Vibrio cholerae* from exogenous attacks by the type 6 secretion system. Proc. Natl. Acad. Sci. USA *115*, 7997–8002. https://doi.org/10.1073/pnas.1808469115.

22. Hersch, S.J., Watanabe, N., Stietz, M.S., Manera, K., Kamal, F., Burkinshaw, B., Lam, L., Pun, A., Li, M., Savchenko, A., et al. (2020). Envelope stress responses defend against type six secretion system attacks independently of immunity proteins. Nat. Microbiol. *5*, 706–714. https://doi.org/10.1038/s41564-020-0672-6.

23. Flaugnatti, N., Isaac, S., Lemos Rocha, L.F., Stutzmann, S., Rendueles, O., Stoudmann, C., Vesel, N., Garcia-Garcera, M., Buffet, A., Sana, T.G., et al. (2021). Human commensal gut proteobacteria withstand type VI secretion attacks through immunity protein-independent mechanisms. Nat. Commun. *12*, 5751. https://doi.org/10.1038/s41467-021-26041-0.

24. Basler, M., Ho, B.T., and Mekalanos, J.J. (2013). Tit-for-Tat: Type VI secretion system counterattack during bacterial cell-cell interactions. Cell *152*, 884–894. https://doi.org/10.1016/j.cell.2013.01.042.

25. Guillemette, R., Ushijima, B., Jalan, M., Häse, C.C., and Azam, F. (2020). Insight into the resilience and susceptibility of marine bacteria to T6SS attack by *Vibrio cholerae* and *Vibrio coralliilyticus*. PLoS One *15*, e0227864. https://doi.org/10.1371/journal.pone.0227864.

26. Sorroche, F.G., Spesia, M.B., Zorreguieta, A., and Giordano, W. (2012). A positive correlation between bacterial autoaggregation and biofilm formation in native *Sinorhizobium meliloti* isolates from Argentina. Appl. Environ. Microbiol. *78*, 4092–4101. https://doi.org/10.1128/AEM.07826-11.

27. Kragh, K.N., Hutchison, J.B., Melaugh, G., Rodesney, C., Roberts, A.E.L., Irie, Y., Jensen, P.Ø., Diggle, S.P., Allen, R.J., Gordon, V., et al. (2016). Role of multicellular aggregates in biofilm formation. mBio *7*, e00237. https://doi.org/10.1128/mBio.00237-16.

28. Alhede, M., Lorenz, M., Fritz, B.G., Jensen, P.Ø., Ring, H.C., Bay, L., and Bjarnsholt, T. (2020). Bacterial aggregate size determines phagocytosis efficiency of polymorphonuclear leukocytes. Med. Microbiol. Immunol. *209*, 669–680. https://doi.org/10.1007/s00430-020-00691-1.

29. Caceres, S.M., Malcolm, K.C., Taylor-Cousar, J.L., Nichols, D.P., Saavedra, M.T., Bratton, D.L., Moskowitz, S.M., Burns, J.L., and Nick, J.A. (2014). Enhanced in vitro formation and antibiotic resistance of nonattached *Pseudomonas aeruginosa* aggregates through incorporation of neutrophil products. Antimicrob. Agents Chemother. *58*, 6851–6860. https://doi.org/10.1128/AAC.03514-14.

30. Corno, G., Coci, M., Giardina, M., Plechuk, S., Campanile, F., and Stefani, S. (2014). Antibiotics promote aggregation within aquatic bacterial communities. Front. Microbiol. *5*, 297. https://doi.org/10.3389/fmicb.2014.00297.

31. Trunk, T., Khalil, H.S., and Leo, J.C. (2018). Bacterial autoaggregation. AIMS Microbiol. *4*, 140–164. https://doi.org/10.3934/microbiol.2018.1.140.

32. Ligthart, K., Belzer, C., de Vos, W.M., and Tytgat, H.L.P. (2020). Bridging bacteria and the gut: functional aspects of Type IV pili. Trends Microbiol. *28*, 340–348. https://doi.org/10.1016/j.tim.2020.02.003.

33. Ellison, C.K., Whitfield, G.B., and Brun, Y.V. (2022). Type IV Pili: dynamic bacterial nanomachines. FEMS Microbiol. Rev. *46*, fuab053. https://doi.org/10.1093/femsre/fuab053.

34. Craig, L., Forest, K.T., and Maier, B. (2019). Type IV pili: dynamics, biophysics and functional consequences. Nat. Rev. Microbiol. *17*, 429–440. https://doi.org/10.1038/s41579-019-0195-4.

35. Taylor, R.K., Miller, V.L., Furlong, D.B., and Mekalanos, J.J. (1987). Use of phoA gene fusions to identify a pilus colonization factor coordinately regulated with cholera toxin. Proc. Natl. Acad. Sci. USA *84*, 2833–2837. https://doi.org/10.1073/pnas.84.9.2833.

36. O'Toole, G.A., and Kolter, R. (1998). Flagellar and twitching motility are necessary for *Pseudomonas aeruginosa* biofilm development. Mol. Microbiol. *30*, 295–304. https://doi.org/10.1046/j.1365-2958.1998.01062.x.

37. Carbonnelle, E., Helaine, S., Nassif, X., and Pelicic, V. (2006). A systematic genetic analysis in *Neisseria meningitidis* defines the Pil proteins required for assembly, functionality, stabilization and export of type IV pili. Mol. Microbiol. *61*, 1510–1522. https://doi.org/10.1111/j.1365-2958.2006.05341.x.

38. Owen, P., Meehan, M., de Loughry-Doherty, H., and Henderson, I. (1996). Phase-variable outer membrane proteins in *Escherichia coli*. FEMS Immunol. Med. Microbiol. *16*, 63–76. https://doi.org/10.1111/j.1574-695X.1996.tb00124.x.

39. Altindis, E., Dong, T., Catalano, C., and Mekalanos, J. (2015). Secretome analysis of *Vibrio cholerae* Type VI secretion system reveals a new effector-immunity pair. mBio *6*, e00075. https://doi.org/10.1128/mBio.00075-15.

40. Labbate, M., Orata, F.D., Petty, N.K., Jayatilleke, N.D., King, W.L., Kirchberger, P.C., Allen, C., Mann, G., Mutreja, A., Thomson, N.R., et al. (2016). A genomic island in *Vibrio cholerae* with VPI-1 site-specific recombination characteristics contains CRISPR-Cas and type VI secretion modules. Sci. Rep. *6*, 36891. https://doi.org/10.1038/srep36891.

41. Crisan, C.V., Chande, A.T., Williams, K., Raghuram, V., Rishishwar, L., Steinbach, G., Watve, S.S., Yunker, P., Jordan, I.K., and Hammer, B.K. (2019). Analysis of *Vibrio cholerae* genomes identifies new type VI secretion system gene clusters. Genome Biol. *20*, 163. https://doi.org/10.1186/s13059-019-1765-5.

42. Meibom, K.L., Blokesch, M., Dolganov, N.A., Wu, C.Y., and Schoolnik, G.K. (2005). Chitin induces natural competence in *Vibrio cholerae*. Science *310*, 1824–1827. https://doi.org/10.1126/science.1120096.

43. Borgeaud, S., Metzger, L.C., Scrignari, T., and Blokesch, M. (2015). The type VI secretion system of *Vibrio cholerae* fosters horizontal gene transfer. Science *347*, 63–67. https://doi.org/10.1126/science.1260064.

44. Matthey, N., Stutzmann, S., Stoudmann, C., Guex, N., Iseli, C., and Blokesch, M. (2019). Neighbor predation linked to natural competence fosters the transfer of large genomic regions in *Vibrio cholerae*. eLife *8*, e48212. https://doi.org/10.7554/eLife.48212.

45. Watve, S.S., Thomas, J., and Hammer, B.K. (2015). CytR is a global positive regulator of competence, Type VI secretion, and chitinases in *Vibrio cholerae*. PLoS One *10*, e0138834. https://doi.org/10.1371/journal.pone.0138834.

46. Jaskólska, M., Stutzmann, S., Stoudmann, C., and Blokesch, M. (2018). QstR-dependent regulation of natural competence and type VI secretion in *Vibrio cholerae*. Nucleic Acids Res. *46*, 10619–10634. https://doi.org/10.1093/nar/gky717.

47. Unterweger, D., Kitaoka, M., Miyata, S.T., Bachmann, V., Brooks, T.M., Moloney, J., Sosa, O., Silva, D., Duran-Gonzalez, J., Provenzano, D., et al. (2012). Constitutive Type VI secretion system expression gives *Vibrio cholerae* intra- and interspecific competitive advantages. PLoS One *7*, e48320. https://doi.org/10.1371/journal.pone.0048320.

48. Bernardy, E.E., Turnsek, M.A., Wilson, S.K., Tarr, C.L., and Hammer, B.K. (2016). Diversity of clinical and environmental isolates of *Vibrio cholerae* in natural transformation and contact-dependent bacterial killing indicative of Type VI secretion system activity. Appl. Environ. Microbiol. *82*, 2833–2842. https://doi.org/10.1128/AEM.00351-16.

49. Drebes Dörr, N.C., Proutière, A., Jaskólska, M., Stutzmann, S., Bader, L., and Blokesch, M. (2022). Single nucleotide polymorphism determines constitutive versus inducible type VI secretion in *Vibrio cholerae*. ISME J. *16*, 1868–1872. https://doi.org/10.1038/s41396-022-01234-7.

50. Ng, S.L., Kammann, S., Steinbach, G., Hoffmann, T., Yunker, P.J., and Hammer, B.K. (2022). Evolution of a *cis*-acting SNP that controls Type VI secretion in *Vibrio cholerae*. mBio *13*, e0042222. https://doi.org/10.1128/mbio.00422-22.

51. Adams, D.W., Stutzmann, S., Stoudmann, C., and Blokesch, M. (2019). DNA-uptake pili of *Vibrio cholerae* are required for chitin colonization and capable of kin recognition via sequence-specific self-interaction. Nat. Microbiol. *4*, 1545–1557. https://doi.org/10.1038/s41564-019-0479-5.

52. Giltner, C.L., Nguyen, Y., and Burrows, L.L. (2012). Type IV Pilin proteins: versatile molecular modules. Microbiol. Mol. Biol. Rev. *76*, 740–772. https://doi.org/10.1128/MMBR.00035-12.

53. Aagesen, A.M., and Häse, C.C. (2012). Sequence analyses of Type IV pili from *Vibrio cholerae*, *Vibrio parahaemolyticus*, and *Vibrio vulnificus*. Microb. Ecol. *64*, 509–524. https://doi.org/10.1007/s00248-012-0021-2.

54. Ronish, L.A., Lillehoj, E., Fields, J.K., Sundberg, E.J., and Piepenbrink, K.H. (2019). The structure of PilA from *Acinetobacter baumannii* AB5075 suggests a mechanism for functional specialization in *Acinetobacter* type IV pili. J. Biol. Chem. *294*, 218–230. https://doi.org/10.1074/jbc.RA118.005814.

55. Custodio, R., Ford, R.M., Ellison, C.J., Liu, G., Mickute, G., Tang, C.M., and Exley, R.M. (2021). Type VI secretion system killing by commensal *Neisseria* is influenced by expression of type four pili. eLife *10*, e63755. https://doi.org/10.7554/eLife.63755.

56. Pukatzki, S., Ma, A.T., Sturtevant, D., Krastins, B., Sarracino, D., Nelson, W.C., Heidelberg, J.F., and Mekalanos, J.J. (2006). Identification of a conserved bacterial protein secretion system in *Vibrio cholerae* using the *Dictyostelium* host model system. Proc. Natl. Acad. Sci. USA *103*, 1528–1533. https://doi.org/10.1073/pnas.0510322103.

57. Hélaine, S., Carbonnelle, E., Prouvensier, L., Beretti, J.-L., Nassif, X., and Pelicic, V. (2005). PilX, a pilus-associated protein essential for bacterial aggregation, is a key to pilus-facilitated attachment of *Neisseria meningitidis* to human cells. Mol. Microbiol. *55*, 65–77. https://doi.org/10.1111/j.1365-2958.2004.04372.x.

58. Speare, L., Woo, M., Bultman, K.M., Mandel, M.J., Wollenberg, M.S., and Septer, A.N. (2021). Host-Like Conditions Are Required for T6SS-Mediated Competition among Vibrio fischeri Light Organ Symbionts. mSphere *6*, e0128820. https://doi.org/10.1128/mSphere.01288-20.

59. Ringel, P.D., Hu, D., and Basler, M. (2017). The role of Type VI secretion system effectors in target cell lysis and subsequent horizontal gene transfer. Cell Rep. *21*, 3927–3940. https://doi.org/10.1016/j.celrep.2017.12.020.

60. Ting, S.-Y., Martínez-García, E., Huang, S., Bertolli, S.K., Kelly, K.A., Cutler, K.J., Su, E.D., Zhi, H., Tang, Q., Radey, M.C., et al. (2020). Targeted depletion of bacteria from mixed populations by programmable adhesion with antagonistic competitor cells. Cell Host Microbe *28*, 313–321.e6. https://doi.org/10.1016/j.chom.2020.05.006.

61. Kirchberger, P.C., Unterweger, D., Provenzano, D., Pukatzki, S., and Boucher, Y. (2017). Sequential displacement of Type VI Secretion System effector genes leads to evolution of diverse immunity gene arrays in *Vibrio cholerae*. Sci. Rep. *7*, 45133. https://doi.org/10.1038/srep45133.

62. Salomon, D., Klimko, J.A., Trudgian, D.C., Kinch, L.N., Grishin, N.V., Mirzaei, H., and Orth, K. (2015). Type VI secretion system toxins horizontally shared between marine bacteria. PLoS Pathog. *11*, e1005128. https://doi.org/10.1371/journal.ppat.1005128.

63. Wielert, I., Kraus-Römer, S., Volkmann, T.E., Craig, L., Higgins, P.G., and Maier, B. (2023). Antigenic variation impacts gonococcal lifestyle and antibiotic tolerance by modulating interbacterial forces. Preprint at bioRxiv. https://doi.org/10.1101/2023.07.06.548055.

64. Smith, W.P.J., Vettiger, A., Winter, J., Ryser, T., Comstock, L.E., Basler, M., and Foster, K.R. (2020). The evolution of the type VI secretion system as a disintegration weapon. PLoS Biol. *18*, e3000720. https://doi.org/10.1371/journal.pbio.3000720.

65. Smith, W.P.J., Brodmann, M., Unterweger, D., Davit, Y., Comstock, L.E., Basler, M., and Foster, K.R. (2020). The evolution of tit-for-tat in bacteria via the type VI secretion system. Nat. Commun. *11*, 5395. https://doi.org/10.1038/s41467-020-19017-z.

66. Jude, B.A., and Taylor, R.K. (2011). The physical basis of type 4 pilus-mediated microcolony formation by *Vibrio cholerae* O1. J. Struct. Biol. *175*, 1–9. https://doi.org/10.1016/j.jsb.2011.04.008.

67. Yildiz, F.H., and Schoolnik, G.K. (1998). Role of rpoS in stress survival and virulence of *Vibrio cholerae*. J. Bacteriol. *180*, 773–784. https://doi.org/10.1128/JB.180.4.773-784.1998.

68. De Souza Silva, O., and Blokesch, M. (2010). Genetic manipulation of *Vibrio cholerae* by combining natural transformation with FLP recombination. Plasmid *64*, 186–195. https://doi.org/10.1016/j.plasmid.2010.08.001.

69. Simon, R., Priefer, U., and Pühler, A. (1983). A broad Host Range Mobilization System for In Vivo Genetic Engineering: Transposon Mutagenesis in Gram Negative Bacteria. Nat. Biotechnol. *1*, 784–791. https://doi.org/10.1038/nbt1183-784.

70. Matthey, N., Drebes Dörr, N.C., and Blokesch, M. (2018). Long-read-based genome sequences of pandemic and environmental *Vibrio cholerae* Strains. Microbiol. Resour. Announc. *7*. e01574–e01518. https://doi.org/10.1128/MRA.01574-18.

71. Murase, K., Arakawa, E., Izumiya, H., Iguchi, A., Takemura, T., Kikuchi, T., Nakagawa, I., Thomson, N.R., Ohnishi, M., and Morita, M. (2022). Genomic dissection of the *Vibrio cholerae* O-serogroup global reference strains: reassessing our view of diversity and plasticity between two chromosomes. Microb. Genom. *8*, mgen000860. https://doi.org/10.1099/mgen.0.000860.

72. Azarian, T., Ali, A., Johnson, J.A., Jubair, M., Cella, E., Ciccozzi, M., Nolan, D.J., Farmerie, W., Rashid, M.H., Sinha-Ray, S., et al. (2016). Non-toxigenic environmental *Vibrio cholerae* O1 strain from Haiti provides evidence of pre-pandemic cholera in Hispaniola. Sci. Rep. *6*, 36115. https://doi.org/10.1038/srep36115.

73. Bina, R.F., Bina, J.E., and Weng, Y. (2020). Genome sequence of *Vibrio cholerae* Strain RFB16, isolated from North Park lake in allegheny county, Pennsylvania. Microbiol. Resour. Announc. *9*, e00111–e00120. https://doi.org/10.1128/MRA.00111-20.

74. Dorman, M.J., Kane, L., Domman, D., Turnbull, J.D., Cormie, C., Fazal, M.-A., Goulding, D.A., Russell, J.E., Alexander, S., and Thomson, N.R. (2019). The history, genome and biology of NCTC 30: a non-pandemic *Vibrio cholerae* isolate from World War one. Proc. Biol. Sci. *286*, 20182025. https://doi.org/10.1098/rspb.2018.2025.

75. Katz, L.S., Turnsek, M., Kahler, A., Hill, V.R., Boyd, E.F., and Tarr, C.L. (2014). Draft genome sequence of environmental *Vibrio cholerae* 2012EL-1759 with similarities to the *V. cholerae* O1 classical biotype. Genome Announc. *2*. e00617–e00614. https://doi.org/10.1128/genomeA.00617-14.

76. Bishop-Lilly, K.A., Johnson, S.L., Verratti, K., Luu, T., Khiani, A., Awosika, J., Mokashi, V.P., Chain, P.S.G., and Sozhamannan, S. (2014). Genome sequencing of 15 clinical *Vibrio* isolates, including 13 non-O1/Non-O139 serogroup strains. Genome Announc. *2*. e00893–e00814. https://doi.org/10.1128/genomeA.00893-14.

77. Khatri, I., Mahajan, S., Dureja, C., Subramanian, S., and Raychaudhuri, S. (2013). Evidence of a new metabolic capacity in an emerging diarrheal pathogen: lessons from the draft genomes of *Vibrio fluvialis* strains PG41 and I21563. Gut Pathog. *5*, 20. https://doi.org/10.1186/1757-4749-5-20.

78. Dziejman, M., Serruto, D., Tam, V.C., Sturtevant, D., Diraphat, P., Faruque, S.M., Rahman, M.H., Heidelberg, J.F., Decker, J., Li, L., et al. (2005). Genomic characterization of non-O1, non-O139 *Vibrio cholerae* reveals genes for a type III secretion system. Proc. Natl. Acad. Sci. USA *102*, 3465–3470. https://doi.org/10.1073/pnas.0409918102.

79. Bao, Y., Lies, D.P., Fu, H., and Roberts, G.P. (1991). An improved Tn7-based system for the single-copy insertion of cloned genes into chromosomes of gram-negative bacteria. Gene *109*, 167–168. https://doi.org/10.1016/0378-1119(91)90604-A.

80. Lo Scrudato, M., and Blokesch, M. (2012). The regulatory network of natural competence and transformation of *Vibrio cholerae*. PLoS Genet. *8*, e1002778. https://doi.org/10.1371/journal.pgen.1002778.

81. Meibom, K.L., Li, X.B., Nielsen, A.T., Wu, C.-Y., Roseman, S., and Schoolnik, G.K. (2004). The *Vibrio cholerae* chitin utilization program. Proc. Natl. Acad. Sci. USA *101*, 2524–2529. https://doi.org/10.1073/pnas.0308707101.

82. Schindelin, J., Arganda-Carreras, I., Frise, E., Kaynig, V., Longair, M., Pietzsch, T., Preibisch, S., Rueden, C., Saalfeld, S., Schmid, B., et al. (2012). Fiji: an open-source platform for biological-image analysis. Nat. Methods *9*, 676–682. https://doi.org/10.1038/nmeth.2019.

83. Tatusova, T., DiCuccio, M., Badretdin, A., Chetvernin, V., Nawrocki, E.P., Zaslavsky, L., Lomsadze, A., Pruitt, K.D., Borodovsky, M., and Ostell, J. (2016). NCBI prokaryotic genome annotation pipeline. Nucleic Acids Res. *44*, 6614–6624. https://doi.org/10.1093/nar/gkw569.

84. Gautreau, G., Bazin, A., Gachet, M., Planel, R., Burlot, L., Dubois, M., Perrin, A., Médigue, C., Calteau, A., Cruveiller, S., et al. (2020). PPanGGOLiN: depicting microbial diversity via a partitioned pangenome graph. PLoS Comput. Biol. *16*, e1007732. https://doi.org/10.1371/journal.pcbi.1007732.

85. Minh, B.Q., Schmidt, H.A., Chernomor, O., Schrempf, D., Woodhams, M.D., von Haeseler, A., and Lanfear, R. (2020). IQ-TREE 2: New models and efficient methods for phylogenetic inference in the genomic era. Mol. Biol. Evol. *37*, 1530–1534. https://doi.org/10.1093/molbev/msaa015.

86. R Core Team (2021). R: A Language and Environment for Statistical Computing (R Foundation for Statistical Computing). https://www.R-project.org.

87. Heibl, C. (2008). PHYLOCH: R language tree plotting tools and interfaces to diverse phylogenetic software packages. http://www.christophheibl.de/Rpackages.html.

88. Wee, S., and Wilkinson, B.J. (1988). Increased outer membrane ornithine-containing lipid and lysozyme penetrability of *Paracoccus denitrificans* grown in a complex medium deficient in divalent cations. J. Bacteriol. *170*, 3283–3286. https://doi.org/10.1128/jb.170.7.3283-3286.1988.

89. Tang, M.-X., Pei, T.-T., Xiang, Q., Wang, Z.-H., Luo, H., Wang, X.-Y., Fu, Y., and Dong, T. (2022). Abiotic factors modulate interspecies competition mediated by the type VI secretion system effectors in *Vibrio cholerae*. ISME J. *16*, 1765–1775. https://doi.org/10.1038/s41396-022-01228-5.

90. Mewes, A., Langer, G., de Nooijer, L.J., Bijma, J., and Reichart, G.-J. (2014). Effect of different seawater Mg2+ concentrations on calcification in two benthic foraminifers. Mar. Micropaleontol. *113*, 56–64. https://doi.org/10.1016/j.marmicro.2014.09.003.

91. LaCourse, K.D., Peterson, S.B., Kulasekara, H.D., Radey, M.C., Kim, J., and Mougous, J.D. (2018). Conditional toxicity and synergy drive diversity among antibacterial effectors. Nat. Microbiol. *3*, 440–446. https://doi.org/10.1038/s41564-018-0113-y.

92. Lambertsen, L., Sternberg, C., and Molin, S. (2004). Mini-Tn7 transposons for site-specific tagging of bacteria with fluorescent proteins. Environ. Microbiol. *6*, 726–732. https://doi.org/10.1111/j.1462-2920.2004.00605.x.

93. Sambrook, J., Fritsch, E.F., and Maniatis, T. (1989). Molecular Cloning: a Laboratory Manual (Cold Spring Harbor Laboratory Press).

94. Marvig, R.L., and Blokesch, M. (2010). Natural transformation of *Vibrio cholerae* as a tool - Optimizing the procedure. BMC Microbiol. *10*, 155. https://doi.org/10.1186/1471-2180-10-155.

95. Blokesch, M. (2012). TransFLP — A method to genetically modify *Vibrio cholerae* based on natural transformation and FLP-recombination. J. Vis. Exp. e3761. https://doi.org/10.3791/3761.

96. Jaskólska, M., and Gerdes, K. (2015). CRP-dependent positive autoregulation and proteolytic degradation regulate competence activator Sxy of *Escherichia coli*. Mol. Microbiol. *95*, 833–845. https://doi.org/10.1111/mmi.12901.

97. Jaskólska, M., Adams, D.W., and Blokesch, M. (2022). Two defence systems eliminate plasmids from seventh pandemic *Vibrio cholerae*. Nature *604*, 323–329. https://doi.org/10.1038/s41586-022-04546-y.

98. Taylor, G.I. (1922). Diffusion by continuous movements. Proc. Lond. Math. Soc. *s2–20*, 196–212. https://doi.org/10.1112/plms/s2-20.1.196.

99. Tchen, C.M. (1959). Diffusion of particles in turbulent flow. Adv. Geophys. *6*, 165–174. https://doi.org/10.1016/S0065-2687(08)60103-X.

100. Roberts, P.J.W., and Webster, D.R. (2002). Turbulent diffusion. In Environmental Fluid Mechanics Theories and Application, H.H. Shen, A.H.D. Cheng, K.-H. Wang, M.H. Teng, and C.C.K. Liu, eds. (ASCE), pp. 7–46.

101. Lovely, P.S., and Dahlquist, F.W. (1975). Statistical measures of bacterial motility and chemotaxis. J. Theor. Biol. *50*, 477–496. https://doi.org/10.1016/0022-5193(75)90094-6.

102. Lemos Rocha, L.F., Peters, K., Biboy, J., Depelteau, J.S., Briegel, A., Vollmer, W., and Blokesch, M. (2022). The VarA-CsrA regulatory pathway influences cell shape in *Vibrio cholerae*. PLoS Genet. *18*, e1010143. https://doi.org/10.1371/journal.pgen.1010143.

103. Grognot, M., Mittal, A., Mah'moud, M., and Taute, K.M. (2021). *Vibrio cholerae* motility in aquatic and mucus-mimicking environments. Appl.

Environ. Microbiol. *87*, e0129321. https://doi.org/10.1128/AEM.01293-21.

104. Landau, D.P., and Binder, K. (2021). A Guide to Monte Carlo Simulations in Statistical Physics (Cambridge University Press). https://doi.org/10.1017/9781108780346.

105. Lee, C.-K., Wang, Y.-M., Huang, L.-S., and Lin, S. (2007). Atomic force microscopy: determination of unbinding force, off rate and energy barrier for protein–ligand interaction. Micron *38*, 446–461. https://doi.org/10.1016/j.micron.2006.06.014.

106. Thomen, P., Valentin, J.D.P., Bitbol, A.-F., and Henry, N. (2020). Spatiotemporal pattern formation in *E. coli* biofilms explained by a simple physical energy balance. Soft Matter *16*, 494–504. https://doi.org/10.1039/c9sm01375j.

107. Bittner, E., and Janke, W. (2008). A boundary field induced first-order transition in the 2D Ising model: numerical study. J. Phys. A: Math. Theor. *41*, 395001. https://doi.org/10.1088/1751-8113/41/39/395001.

108. Blöte, H.W.J., Heringa, J.R., and Tsypin, M.M. (2000). Three-dimensional Ising model in the fixed-magnetization ensemble: A Monte Carlo study. Phys. Rev. E Stat. Phys. Plasmas Fluids Relat. Interdiscip. Topics *62*, 77–82. https://doi.org/10.1103/PhysRevE.62.77.

109. Alston, H., Parry, A.O., Voituriez, R., and Bertrand, T. (2022). Intermittent attractive interactions lead to microphase separation in nonmotile active matter. Phys. Rev. E *106*, 034603. https://doi.org/10.1103/PhysRevE.106.034603.

110. Kuan, H.-S., Pönisch, W., Jülicher, F., and Zaburdaev, V. (2021). Continuum theory of active phase separation in cellular aggregates. Phys. Rev. Lett. *126*, 018102. https://doi.org/10.1103/PhysRevLett.126.018102.

111. Bonazzi, D., Lo Schiavo, V., Machata, S., Djafer-Cherif, I., Nivoit, P., Manriquez, V., Tanimoto, H., Husson, J., Henry, N., Chaté, H., et al. (2018). Intermittent pili-mediated forces fluidize *Neisseria meningitidis* aggregates promoting vascular colonization. Cell *174*, 143–155.e16. https://doi.org/10.1016/j.cell.2018.04.010.

112. Kalyaanamoorthy, S., Minh, B.Q., Wong, T.K.F., von Haeseler, A., and Jermiin, L.S. (2017). ModelFinder: fast model selection for accurate phylogenetic estimates. Nat. Methods *14*, 587–589. https://doi.org/10.1038/nmeth.4285.

Please cite this article in press as: Otto et al., Interactions between pili affect the outcome of bacterial competition driven by the type VI secretion system, Current Biology (2024), https://doi.org/10.1016/j.cub.2024.04.041

STAR★METHODS

KEY RESOURCES TABLE

REAGENT or RESOURCE	SOURCE	IDENTIFIER
Bacterial and virus strains		
A1552 (*Vibrio cholerae* O1 El Tor Inaba strain; Rif^R)	Yildiz and Schoolnik[67]	A1552 (GC#1)
A1552 deleted for *lacZ*; Rif^R	De Souza Silva and Blokesch[68]	A1552Δ*lacZ*::FRT (GC#1208)
Δ*VC1807*::FRT-Kan^R-FRT-PA1/04/03-$mCherry_{op13}$; Kan^R cassette (*aph*) and *mCherry*, which has been codon changed to enrich the A/T content in the first 13 codons of the 5' region; *mCherry* is preceded by the constitutive P_{lac}-derivative promoter, PA1/04/03; Rif^R	This paper	A1552-KanR-mCherry (GC#9700)
Δ*VC1807*::FRT-$Spec^R$-FRT-PA1/04/03-sfGFP; $Spec^R$ (*aad9*) cassette and *sfGFP*; *sfGFP* is preceded by the constitutive P_{lac}-derivative promoter, PA1/04/03; Rif^R	This paper	A1552-SpecR-sfGFP (GC#9695)
A1552Δ*VC1418-19*::FRT, Δ*VCA0020-21*::FRT, Δ*VCA0123-24*::FRT, Δ*VCA0285-86*::FRT	This paper	A1552-Δ4E/I (GC#9523)
A1552-Tn*tfoX*, Δ*pilT*; Rif^R	This paper	A1552-Tn*tfoX*, Δ*pilT* (GC#10495)
A1552-Tn*tfoX*, Δ*pilT*, Δ*pilA*; Rif^R	This paper	A1552-Tn*tfoX*, Δ*pilT*, Δ*pilA* (GC#10496)
Tn*tfoX*, Δ*pilT*, Δ*VC1418-19*::FRT, Δ*VCA0020-21*::FRT, Δ*VCA0123-24*::FRT, Δ*VCA0285-86*::FRT, Δ*VC1807*::FRT-$Spec^R$-FRT-PA1/04/03-sfGFP; Rif^R	This paper	A1552-Tn*tfoX*, Δ*pilT*, Δ4E/I, SpecR-sfGFP (GC#10501)
Tn*tfoX*, Δ*pilT*, Δ*VC1807*::FRT-Kan^R-FRT-PA1/04/03-$mCherry_{op13}$; Rif^R	This paper	A1552-Tn*tfoX*, Δ*pilT*, KanR-mCherry (GC#10497)
Tn*tfoX*, Δ*pilT*, Δ*pilA*, Δ*VC1418-19*::FRT, Δ*VCA0020-21*::FRT, Δ*VCA0123-24*::FRT, Δ*VCA0285-86*::FRT, Δ*VC1807*::FRT-$Spec^R$-FRT-PA1/04/03-sfGFP; Rif^R	This paper	A1552-Tn*tfoX*, Δ*pilT*, Δ*pilA*, Δ4E/I, SpecR-sfGFP (GC#10498)
Tn*tfoX*, Δ*pilT*, Δ*pilA*, Δ*VC1807*::FRT-Kan^R-FRT-PA1/04/03-$mCherry_{op13}$; Rif^R	This paper	A1552-Tn*tfoX*, Δ*pilT*, Δ*pilA*, KanR-mCherry (GC#10500)
Tn*tfoX*, Δ*pilT*, Δ*vasK*, Δ*VC1807*::FRT-Kan^R-FRT-PA1/04/03-$mCherry_{op13}$; Rif^R	This paper	A1552-Tn*tfoX*, Δ*pilT*, Δ*vasK*, KanR-mCherry (GC#10499)
Tn*tfoX*, Δ*pilT*, Δ*pilA*, Δ*vasK*, Δ*VC1807*::FRT-Kan^R-FRT-PA1/04/03-$mCherry_{op13}$; Rif^R	This paper	A1552-Tn*tfoX*, Δ*pilT*, Δ*pilA*, Δ*vasK*, KanR-mCherry (GC#10507)
Tn*tfoX*, Δ*pilT*, *pilA*rep[A1552], Δ*VC1418-19*::FRT, Δ*VCA0020-21*::FRT, Δ*VCA0123-24*::FRT, Δ*VCA0285-86*::FRT, Δ*VC1807*::FRT-$Spec^R$-FRT-PA1/04/03-sfGFP; Rif^R	This paper	A1552-Tn*tfoX*, Δ*pilT*, *pilA*rep[A1552], Δ4E/I, SpecR-sfGFP (GC#10504)
Tn*tfoX*, Δ*pilT*, *pilA*rep[A1552], Δ*VC1807*::FRT-Kan^R-FRT-PA1/04/03-$mCherry_{op13}$; Rif^R	This paper	A1552-Tn*tfoX*, Δ*pilT*, *pilA*rep[A1552], KanR-mCherry (GC#10508)
Tn*tfoX*, Δ*pilT*, *pilA*rep[SP6G], Δ*VC1418-19*::FRT, Δ*VCA0020-21*::FRT, Δ*VCA0123-24*::FRT, Δ*VCA0285-86*::FRT, Δ*VC1807*::FRT-$Spec^R$-FRT-PA1/04/03-sfGFP; Rif^R	This paper	A1552-Tn*tfoX*, Δ*pilT*, *pilA*rep[SP6G], Δ4E/I, SpecR-sfGFP (GC#10505)
Tn*tfoX*, Δ*pilT*, *pilA*rep[SP6G], Δ*VC1807*::FRT-Kan^R-FRT-PA1/04/03-$mCherry_{op13}$; Rif^R	This paper	A1552-Tn*tfoX*, Δ*pilT*, *pilA*rep[SP6G], KanR-mCherry (GC#10522)
Tn*tfoX*, Δ*pilT*, *pilA*rep[SP7G], Δ*VC1418-19*::FRT, Δ*VCA0020-21*::FRT, Δ*VCA0123-24*::FRT, Δ*VCA0285-86*::FRT, Δ*VC1807*::FRT-$Spec^R$-FRT-PA1/04/03-sfGFP; Rif^R	This paper	A1552-Tn*tfoX*, Δ*pilT*, *pilA*rep[SP7G], Δ4E/I, SpecR-sfGFP (GC#10510)
Tn*tfoX*, Δ*pilT*, *pilA*rep[SP7G], Δ*VC1807*::FRT-Kan^R-FRT-PA1/04/03-$mCherry_{op13}$; Rif^R	This paper	A1552-Tn*tfoX*, Δ*pilT*, *pilA*rep[SP7G], KanR-mCherry (GC#10518)

(*Continued on next page*)

Please cite this article in press as: Otto et al., Interactions between pili affect the outcome of bacterial competition driven by the type VI secretion system, Current Biology (2024), https://doi.org/10.1016/j.cub.2024.04.041

CellPress
OPEN ACCESS

Continued

REAGENT or RESOURCE	SOURCE	IDENTIFIER
Tn*tfoX*, Δ*pilT*, *pilA*rep[L6G], Δ*VC1418-19*::FRT, Δ*VCA0020-21*::FRT, Δ*VCA0123-24*::FRT, Δ*VCA0285-86*::FRT, Δ*VC1807*::FRT-Spec^R-FRT-PA1/04/03-sfGFP; Rif^R	This paper	A1552-Tn*tfoX*, Δ*pilT*, *pilA*rep[L6G], Δ4E/I, SpecR-sfGFP (GC#10512)
Tn*tfoX*, Δ*pilT*, *pilA*rep[L6G], Δ*VC1807*::FRT-Kan^R-FRT-PA1/04/03-mCherry$_{op13}$; Rif^R	This paper	A1552-Tn*tfoX*, Δ*pilT*, *pilA*rep[L6G], KanR-mCherry (GC#10520)
Tn*tfoX*, Δ*pilT*, *pilA*rep[SA3G], Δ*VC1418-19*::FRT, Δ*VCA0020-21*::FRT, Δ*VCA0123-24*::FRT, Δ*VCA0285-86*::FRT, Δ*VC1807*::FRT-Spec^R-FRT-PA1/04/03-sfGFP; Rif^R	This paper	A1552-Tn*tfoX*, Δ*pilT*, *pilA*rep[SA3G], Δ4E/I, SpecR-sfGFP (GC#10513)
Tn*tfoX*, Δ*pilT*, *pilA*rep[SA3G], Δ*VC1807*::FRT-Kan^R-FRT-PA1/04/03-mCherry$_{op13}$; Rif^R	This paper	A1552-Tn*tfoX*, Δ*pilT*, *pilA*rep[SA3G], KanR-mCherry (GC#10521)
Tn*tfoX*, Δ*pilT*, *pilA*rep[TP], Δ*VC1418-19*::FRT, Δ*VCA0020-21*::FRT, Δ*VCA0123-24*::FRT, Δ*VCA0285-86*::FRT, Δ*VC1807*::FRT-Spec^R-FRT-PA1/04/03-sfGFP; Rif^R	This paper	A1552-Tn*tfoX*, Δ*pilT*, *pilA*rep[TP], Δ4E/I, SpecR-sfGFP (GC#10514)
Tn*tfoX*, Δ*pilT*, *pilA*rep[TP], Δ*VC1807*::FRT-Kan^R-FRT-PA1/04/03-mCherry$_{op13}$; Rif^R	This paper	A1552-Tn*tfoX*, Δ*pilT*, *pilA*rep[TP], KanR-mCherry (GC#10523)
Tn*tfoX*, Δ*pilT*, *pilA*rep[DL4215], Δ*VC1418-19*::FRT, Δ*VCA0020-21*::FRT, Δ*VCA0123-24*::FRT, Δ*VCA0285-86*::FRT, Δ*VC1807*::FRT-Spec^R-FRT-PA1/04/03-sfGFP; Rif^R	This paper	A1552-Tn*tfoX*, Δ*pilT*, *pilA*rep[DL4215], Δ4E/I, SpecR-sfGFP (GC#10515)
Tn*tfoX*, Δ*pilT*, *pilA*rep[DL4215], Δ*VC1807*::FRT-Kan^R-FRT-PA1/04/03-mCherry$_{op13}$; Rif^R	This paper	A1552-Tn*tfoX*, Δ*pilT*, *pilA*rep[DL4215], KanR-mCherry (GC#10524)
Tn*tfoX*, Δ*pilT*, *pilA*rep[1587], Δ*VC1418-19*::FRT, Δ*VCA0020-21*::FRT, Δ*VCA0123-24*::FRT, Δ*VCA0285-86*::FRT, Δ*VC1807*::FRT-Spec^R-FRT-PA1/04/03-sfGFP; Rif^R	This paper	A1552-Tn*tfoX*, Δ*pilT*, *pilA*rep[1587], Δ4E/I, SpecR-sfGFP (GC#10516)
Tn*tfoX*, Δ*pilT*, *pilA*rep[1587], Δ*VC1807*::FRT-Kan^R-FRT-PA1/04/03-mCherry$_{op13}$; Rif^R	This paper	A1552-Tn*tfoX*, Δ*pilT*, *pilA*rep[1587], KanR-mCherry (GC#10525)
Tn*tfoX*, Δ*pilT*, *pilA*rep[SL6Y], Δ*VC1418-19*::FRT, Δ*VCA0020-21*::FRT, Δ*VCA0123-24*::FRT, Δ*VCA0285-86*::FRT, Δ*VC1807*::FRT-Spec^R-FRT-PA1/04/03-sfGFP; Rif^R	This paper	A1552-Tn*tfoX*, Δ*pilT*, *pilA*rep[SL6Y], Δ4E/I, SpecR-sfGFP (GC#10511)
Tn*tfoX*, Δ*pilT*, *pilA*rep[SL6Y], Δ*VC1807*::FRT-Kan^R-FRT-PA1/04/03-mCherry$_{op13}$; Rif^R	This paper	A1552-Tn*tfoX*, Δ*pilT*, *pilA*rep[SL6Y], KanR-mCherry (GC#10519)
Tn*tfoX*, Δ*pilT*, *pilA*rep[DRC186], Δ*VC1418-19*::FRT, Δ*VCA0020-21*::FRT, Δ*VCA0123-24*::FRT, Δ*VCA0285-86*::FRT, Δ*VC1807*::FRT-Spec^R-FRT-PA1/04/03-sfGFP; Rif^R	This paper	A1552-Tn*tfoX*, Δ*pilT*, *pilA*rep[DRC186], Δ4E/I, SpecR-sfGFP (GC#10517)
Tn*tfoX*, Δ*pilT*, *pilA*rep[DRC186], Δ*VC1807*::FRT-Kan^R-FRT-PA1/04/03-mCherry$_{op13}$; Rif^R	This paper	A1552-Tn*tfoX*, Δ*pilT*, *pilA*rep[DRC186], KanR-mCherry (GC#10526)
Tn*tfoX*, Δ*pilT*, *pilA*rep[Sa5Y], Δ*VC1418-19*::FRT, Δ*VCA0020-21*::FRT, Δ*VCA0123-24*::FRT, Δ*VCA0285-86*::FRT, Δ*VC1807*::FRT-Spec^R-FRT-PA1/04/03-sfGFP; Rif^R	This paper	A1552-Tn*tfoX*, Δ*pilT*, *pilA*rep[Sa5Y], Δ4E/I, SpecR-sfGFP (GC#10506)
Tn*tfoX*, Δ*pilT*, *pilA*rep[Sa5Y], Δ*VC1807*::FRT-Kan^R-FRT-PA1/04/03-mCherry$_{op13}$; Rif^R	This paper	A1552-Tn*tfoX*, Δ*pilT*, *pilA*rep[Sa5Y], KanR-mCherry (GC#10528)
Tn*tfoX*, Δ*pilT*, *pilA*rep[V52], Δ*VC1418-19*::FRT, Δ*VCA0020-21*::FRT, Δ*VCA0123-24*::FRT, Δ*VCA0285-86*::FRT, Δ*VC1807*::FRT-Spec^R-FRT-PA1/04/03-sfGFP; Rif^R	This paper	A1552-Tn*tfoX*, Δ*pilT*, *pilA*rep[V52], Δ4E/I, SpecR-sfGFP (GC#10535)
Tn*tfoX*, Δ*pilT*, *pilA*rep[V52], Δ*VC1807*::FRT-Kan^R-FRT-PA1/04/03-mCherry$_{op13}$; Rif^R	This paper	A1552-Tn*tfoX*, Δ*pilT*, *pilA*rep[V52], KanR-mCherry (GC#10529)

(*Continued on next page*)

Please cite this article in press as: Otto et al., Interactions between pili affect the outcome of bacterial competition driven by the type VI secretion system, Current Biology (2024), https://doi.org/10.1016/j.cub.2024.04.041

Continued

REAGENT or RESOURCE	SOURCE	IDENTIFIER
Tn*tfoX*, Δ*pilT*, *pilA*rep[W6G], Δ*VC1418-19*::FRT, Δ*VCA0020-21*::FRT, Δ*VCA0123-24*::FRT, Δ*VCA0285-86*::FRT, Δ*VC1807*::FRT-Spec^R-FRT-PA1/04/03-sfGFP; Rif^R	This paper	A1552-Tn*tfoX*, Δ*pilT*, *pilA*rep[W6G], Δ4E/I, SpecR-sfGFP (GC#10536)
Tn*tfoX*, Δ*pilT*, *pilA*rep[W6G], Δ*VC1807*::FRT-Kan^R-FRT-PA1/04/03-mCherry$_{op13}$; Rif^R	This paper	A1552-Tn*tfoX*, Δ*pilT*, *pilA*rep[W6G], KanR-mCherry (GC#10530)
Tn*tfoX*, Δ*pilT*, *pilA*rep[SA7G], Δ*VC1418-19*::FRT, Δ*VCA0020-21*::FRT, Δ*VCA0123-24*::FRT, Δ*VCA0285-86*::FRT, Δ*VC1807*::FRT-Spec^R-FRT-PA1/04/03-sfGFP; Rif^R	This paper	A1552-Tn*tfoX*, Δ*pilT*, *pilA*rep[SA7G], Δ4E/I, SpecR-sfGFP (GC#10537)
Tn*tfoX*, Δ*pilT*, *pilA*rep[SA7G], Δ*VC1807*::FRT-Kan^R-FRT-PA1/04/03-mCherry$_{op13}$; Rif^R	This paper	A1552-Tn*tfoX*, Δ*pilT*, *pilA*rep[SA7G], KanR-mCherry (GC#10531)
Tn*tfoX*, Δ*pilT*, *pilA*rep[SO5Y], Δ*VC1418-19*::FRT, Δ*VCA0020-21*::FRT, Δ*VCA0123-24*::FRT, Δ*VCA0285-86*::FRT, Δ*VC1807*::FRT-Spec^R-FRT-PA1/04/03-sfGFP; Rif^R	This paper	A1552-Tn*tfoX*, Δ*pilT*, *pilA*rep[SO5Y], Δ4E/I, SpecR-sfGFP (GC#10538)
Tn*tfoX*, Δ*pilT*, *pilA*rep[SO5Y], Δ*VC1807*::FRT-Kan^R-FRT-PA1/04/03-mCherry$_{op13}$; Rif^R	This paper	A1552-Tn*tfoX*, Δ*pilT*, *pilA*rep[SO5Y], KanR-mCherry (GC#10532)
Tn*tfoX*, Δ*pilT*, *pilA*rep[SIO], Δ*VC1418-19*::FRT, Δ*VCA0020-21*::FRT, Δ*VCA0123-24*::FRT, Δ*VCA0285-86*::FRT, Δ*VC1807*::FRT-Spec^R-FRT-PA1/04/03-sfGFP; Rif^R	This paper	A1552-Tn*tfoX*, Δ*pilT*, *pilA*rep[SIO], Δ4E/I, SpecR-sfGFP (GC#10527)
Tn*tfoX*, Δ*pilT*, *pilA*rep[SIO], Δ*VC1807*::FRT-Kan^R-FRT-PA1/04/03-mCherry$_{op13}$; Rif^R	This paper	A1552-Tn*tfoX*, Δ*pilT*, *pilA*rep[SIO], KanR-mCherry (GC#10533)
Tn*tfoX*, Δ*pilT*, *pilA*rep[W10G], Δ*VC1418-19*::FRT, Δ*VCA0020-21*::FRT, Δ*VCA0123-24*::FRT, Δ*VCA0285-86*::FRT, Δ*VC1807*::FRT-Spec^R-FRT-PA1/04/03-sfGFP; Rif^R	This paper	A1552-Tn*tfoX*, Δ*pilT*, *pilA*rep[W10G], Δ4E/I, SpecR-sfGFP (GC#10539)
Tn*tfoX*, Δ*pilT*, *pilA*rep[W10G], Δ*VC1807*::FRT-Kan^R-FRT-PA1/04/03-mCherry$_{op13}$; Rif^R	This paper	A1552-Tn*tfoX*, Δ*pilT*, *pilA*rep[W10G], KanR-mCherry (GC#10534)
Tn*tfoX*, Δ*pilT*, *pilA*rep[A1552], Δ*vasK*, Δ*VC1807*::FRT-Kan^R-FRT-PA1/04/03-mCherry$_{op13}$; Rif^R	This paper	A1552-Tn*tfoX*, Δ*pilT*, *pilA*rep[A1552], Δ*vasK*, KanR-mCherry (GC#10509)
Escherichia coli S17-1 λpir; for cloning and conjugation into *V. cholerae*	Simon et al.[69]	S17-1 λpir (GC#648)
Escherichia coli SM10 λpir; for cloning and conjugation into *V. cholerae*	Simon et al.[69]	SM10 λpir (GC#647)
Chemicals, peptides, and recombinant proteins		
lysogeny broth (LB)	Carl Roth, Switzerland	Cat#X968.3
LB agar	Carl Roth, Switzerland	Cat#X969.3
$CaCl_2$	Sigma-Aldrich	Cat#C5080
$MgCl_2$	PanReac AppliChem ITW Reagents	Cat#A4425
L-arabinose	Carl Roth, Switzerland	Cat#5118.2
Thiosulfate citrate bile salts sucrose (TCBS) agar	Sigma-Aldrich	Cat#86348
sucrose	Sigma-Aldrich	Cat#84100
ampicillin	Carl Roth, Switzerland	Cat#K029.3
gentamicin	Carl Roth, Switzerland	Cat#0233.4
kanamycin	Carl Roth, Switzerland	Cat#T832.4
spectinomycin	Carl Roth, Switzerland	Cat#S9007
5-bromo-4-chloro-3-indolyl β-d-galactopyranoside (X-gal)	PanReac AppliChem ITW Reagents	Cat#A1007
agarose	Carl Roth, Switzerland	Cat#3810.2
phosphate buffered saline (PBS)	Thermo Fisher Scientific	Cat#10010-015
SYTOX Blue Nucleic Acid Stain	Thermo Fisher Scientific	Cat#S11348

(*Continued on next page*)

Continued

REAGENT or RESOURCE	SOURCE	IDENTIFIER
Deposited data		
Original custom code for simulations	This paper	https://github.com/Bitbol-Lab/T4P-T6SS-interplay
Source data containing raw, *p* and growth rate values	This paper	https://doi.org/10.5281/zenodo.10848650
genome of ATCC33655	N/A	GenBank: GCF_001471395.1
genome of A1552	Matthey et al.[70]	GenBank: GCA_003097695.1
genome of SP6G	Drebes Dörr and Blokesch[20]	GenBank: GCA_013357745.1
genome of SP7G	Drebes Dörr and Blokesch[20]	GenBank: GCA_013357765.1
genome of L6G	Drebes Dörr and Blokesch[20]	GenBank: GCA_013357685.1
genome of SA3G	Drebes Dörr and Blokesch[20]	GenBank: GCA_013357885.1
genome of TP	N/A	GenBank: CP137095.1, GenBank: CP137096.1
genome of DL4215	N/A	GenBank: CP137093.1, GenBank: CP137094.1
genome of 1587	N/A	GenBank: CP137097.1,GenBank: CP137098.1
genome of SL6Y	Drebes Dörr and Blokesch[20]	GenBank: GCA_013357725.1
genome of DRC186	N/A	GenBank: GCA_030710345.1
genome of Sa5Y	Matthey et al.[70]	GenBank: GCA_003063885.1
genome of V52	N/A	GenBank: CP137135.1, Genbank: CP137136.1
genome of W6G	Drebes Dörr and Blokesch[20]	GenBank: GCA_013357785.1
genome of SA7G	Drebes Dörr and Blokesch[20]	GenBank: GCA_013357845.1
genome of SO5Y	Drebes Dörr and Blokesch[20]	GenBank: GCA_013357665.1
genome of SIO	N/A	GenBank: JBBHLM000000000.1
genome of W10G	Drebes Dörr and Blokesch[20]	GenBank: GCA_013357605.1
genome of SL5Y	Drebes Dörr and Blokesch[20]	GenBank: GCA_013357645.1
genome of SL4G	Drebes Dörr and Blokesch[20]	GenBank: GCA_013357625.1
genome of W7G	Drebes Dörr and Blokesch[20]	GenBank: GCA_013357805.1
genome of SA10G	Drebes Dörr and Blokesch[20]	GenBank: GCA_013357865.1
genome of E7G	Drebes Dörr and Blokesch[20]	GenBank: GCA_013357825.1
genome of DL4211	N/A	GenBank: CP137091.1, GenBank: CP137092.1
genome of VCSR05	Murase et al.[71]	GenBank: GCA_023168205.1
genome of VCSR0207	Murase et al.[71]	GenBank: GCA_023168105.1
genome of VCSR096	Murase et al.[71]	GenBank: GCA_023168285.1
genome of V130003	N/A	GenBank: GCA_023169825.1
genome of Env-390	Azarian et al.[72]	GenBank: GCF_001854425.1
genome of 2012Env-9	Azarian et al.[72]	GenBank: GCF_000788715.2
genome of VCSR063	Murase et al.[71]	GenBank: GCA_023168245.1
genome of VCSR051	Murase et al.[71]	GenBank: GCA_023168225.1
genome of VCSR0102	Murase et al.[71]	GenBank: GCA_023167925.1
genome of VCSR0162	Murase et al.[71]	GenBank: GCA_023167985.1
genome of RFB16	Bina et al.[73]	GenBank: GCA_008369605.1
genome of VCSR017	Murase et al.[71]	GenBank: GCA_023168045.1
genome of NCTC30	Dorman et al.[74]	GenBank: GCA_900538065.1
genome of VCSR077	Murase et al.[71]	GenBank: GCA_023168265.1
genome of strain20000	N/A	GenBank: GCA_004328575.1
genome of VCSR045	Murase et al.[71]	GenBank: GCA_023168185.1
genome of 2012EL-1759	Katz et al.[75]	GenBank: JNEW00000000.1
genome of HE45	N/A	GenBank: GCF_000279285.1
genome of A325	N/A	GenBank: CWSO00000000.1
genome of 490−93	Bishop-Lilly et al.[76]	GenBank: JIDQ00000000.1
genome of TMA21	N/A	GenBank: ACHY00000000

(*Continued on next page*)

Please cite this article in press as: Otto et al., Interactions between pili affect the outcome of bacterial competition driven by the type VI secretion system, Current Biology (2024), https://doi.org/10.1016/j.cub.2024.04.041

Continued

REAGENT or RESOURCE	SOURCE	IDENTIFIER
genome of MZO-2	N/A	GenBank: GCA_000153985.3
genome of TM11079−80	N/A	GenBank: GCA_000174255.1
genome of PG41	Khatri et al.[77]	GenBank: ASXS00000000.1
genome of VL426	N/A	GenBank: GCF_000174235.1
genome of MZO-3	N/A	GenBank: GCA_000168935.3
genome of AM-19226	Dziejman et al.[78]	GenBank: GCA_000153785.3
genome of S12	Labbate et al.[40]	GenBank: MDST00000000
genome of BC1071	Crisan et al.[41]	GenBank: LT897798.1
Recombinant DNA		
pUX-BF13 - oriR6K, helper plasmid with Tn7 transposition function; Amp^R	Bao et al.[79]	pUX-BF13 (GC#457)
pGP704 with mini-Tn7 carrying *araC* and P_{BAD}-*tfoX*; Amp^R, $Gent^R$ (Tn*tfoX*)	Lo Scrudato and Blokesch[80]	pGP704-mTn*tfoX* (GC#1624)
pGP704-Sac28 suicide vector, *ori*R6K, *sacB*; Amp^R	Meibom et al.[81]	p28 (GC#649)
pGP704-Sac28-Δ*pilA*	Meibom et al.[81]	p28-*pilA* (GC#1050)
pGP704-Sac28-Δ*pilT*	Adams et al.[51]	p28-Δ*pilT* (GC#5959)
pGP704-Sac28-*pilA*rep[A1552]	Adams et al.[51]	p28-*pilA*rep[A1552] (GC#6199)
pGP704-Sac28-*pilA*rep[964; SP6G]	Adams et al.[51]	p28-*pilA*rep[SP6G] (GC#5674)
pGP704-Sac28-*pilA*rep[952; SP7G]	Adams et al.[51]	p28-*pilA*rep[SP7G] (GC#5665)
pGP704-Sac28-*pilA*rep[956; L6G]	Adams et al.[51]	p28-*pilA*rep[L6G] (GC#5666)
pGP704-Sac28-*pilA*rep[957; SA3G]	Adams et al.[51]	p28-*pilA*rep[SA3G] (GC#5667)
pGP704-Sac28-*pilA*rep[999; TP]	Adams et al.[51]	p28-*pilA*rep[TP] (GC#5670)
pGP704-Sac28-*pilA*rep[3079; DL4215]	Adams et al.[51]	p28-*pilA*rep[DL4215] (GC#5671)
pGP704-Sac28-*pilA*rep[3081; 1587]	Adams et al.[51]	p28-*pilA*rep[1587] (GC#5672)
pGP704-Sac28-*pilA*rep[953; SL6Y]	Adams et al.[51]	p28-*pilA*rep[SL6Y] (GC#5673)
pGP704-Sac28-*pilA*rep[2501; DRC186]	Adams et al.[51]	p28-*pilA*rep[DRC186] (GC#5676)
pGP704-Sac28-*pilA*rep[353; Sa5Y]	Adams et al.[51]	p28-*pilA*rep[Sa5Y] (GC#6200)
pGP704-Sac28-*pilA*rep[1510; V52]	Adams et al.[51]	p28-*pilA*rep[V52] (GC#6201)
pGP704-Sac28-*pilA*rep[354; W6G]	Adams et al.[51]	p28-*pilA*rep[W6G] (GC#5664)
pGP704-Sac28-*pilA*rep[959; SA7G]	Adams et al.[51]	p28-*pilA*rep[SA7G] (GC#5668)
pGP704-Sac28-*pilA*rep[960; SO5Y]	Adams et al.[51]	p28-*pilA*rep[SO5Y] (GC#5669)
pGP704-Sac28-*pilA*rep[1000; SIO]	Adams et al.[51]	p28-*pilA*rep[SIO] (GC#5675)
pGP704-Sac28-*pilA*rep[5537; W10G]	Adams et al.[51]	p28-*pilA*rep[W10G] (GC#5677)
pGP704-Sac28-Δ*VCA0285-86*::FRT	This paper	p28-Δ*VCA0285-86*::FRT (GC#10540)
pGP704-Sac28-Δ*VCA0120*	Borgeaud et al.[43]	p28-Δ*vasK* (GC#1124)
pGP704-Sac28-Δ*VC1807*::FRT-Kan^R-FRT-PA1/04/03-$mCherry_{op13}$	This paper	p28-KanR-mCherry (GC#10542)
pGP704-Sac28-Δ*VC1807*::FRT-$Spec^R$-FRT-PA1/04/03-sfGFP	This paper	p28-SpecR-sfGFP (GC#10541)
Software and algorithms		
SnapGene (v. 4.3.11)	Dotmatics	RRID:SCR_015052
Fiji (ImageJ)	Schindelin et al.[82]	RRID:SCR_002285
Zeiss ZEN 2.6 blue edition	Zeiss	RRID:SCR_013672
PGAP 2022-10-03. build6384	Tatusova et al.[83]	RRID:SCR_021329
PPanGGOLiN (v. 1.2.74)	Gautreau et al.[84]	https://github.com/labgem/PPanGGOLiN
iqtree2 (v. 2.2.0)	Minh et al.[85]	RRID:SCR_017254
R (v. 4.2.1)	R Core Team[86]	RRID:SCR_001905

(*Continued on next page*)

Continued

REAGENT or RESOURCE	SOURCE	IDENTIFIER
R ips package (v. 0.0.11)	Heibl[87]	http://www.christophheibl.de/Rpackages.html
makeblastdb command (v. 2.12) in BLAST® Command Line	N/A	https://www.ncbi.nlm.nih.gov/books/NBK279690/
muscle (v. 5.1.osx64)	N/A	RRID:SCR_011812
R bio3d package (v. 2.4-4)	N/A	https://cran.r-project.org/web/packages/bio3d/index.html
pheatmap (v. 1.0.12)	N/A	RRID:SCR_016418
GraphPad Prism (v. 9.1.2)	GraphPad	RRID:SCR_002798

RESOURCE AVAILABILTY

Lead contact

Further information and requests for resources and reagents should be directed to and will be fulfilled by the lead contact, Melanie Blokesch (melanie.blokesch@epfl.ch).

Materials availability

Strains and plasmids generated for this study are available upon request from the lead contact.

Data and code availability

- The source data file containing raw data, *p* values, and growth rates has been deposited in a Zenodo repository (https://doi.org/10.5281/zenodo.10848650).
- All original code has been deposited in a GitHub repository (https://github.com/Bitbol-Lab/T4P-T6SS-interplay).
- Any additional information required to reanalyze the data reported in this paper is available from the lead contact upon request.

EXPERIMENTAL MODEL AND SUBJECT DETAILS

Bacterial strains

The bacterial strains and plasmids used in this study are listed in the key resources table. *V. cholerae* O1 El Tor strain A1552 was used as a genome-sequenced representative of the ongoing seventh cholera pandemic.[67,70]

Growth conditions

Unless otherwise specified, bacteria were cultured in Lysogeny broth (LB) (Carl Roth, Switzerland) or on LB agar plates. The LB medium was supplemented with 1 mM $CaCl_2$ and 5 mM $MgCl_2$ to counteract LB batch-to-batch variability in aggregation[51] (Figure S1C). Indeed, LB medium is often low in divalent cations,[88] and $CaCl_2$ and $MgCl_2$ concentration can be vastly different between batches/different producers.[89] Notably, the $CaCl_2$ and $MgCl_2$ concentrations present in seawater are, on average, considerably higher than those supplemented in this study.[90] Despite this, the addition of divalent cations has been found to have no effect on T6SS secretion, although it has been observed to impact the conditional efficacy of certain T6SS effectors.[89,91]

Cultures were induced with 0.2% L-arabinose to promote the expression of P_{BAD}-driven genes that were carried by a mini-Tn7 transposon[92] integrated on the chromosome. Post-bacterial mating, *Escherichia coli* cells were counter-selected using Thiosulfate citrate bile salts sucrose (TCBS, Sigma-Aldrich) agar. SacB-based counter-selection was carried out on NaCl-free LB agar supplemented with 10% sucrose. Various antibiotics such as ampicillin (Amp, 100 μg ml^{-1}), gentamicin (Gent, 50 μg ml^{-1}), kanamycin (Kan, 75 μg ml^{-1}), or spectinomycin (Spec, 200 μg ml^{-1}) were added when necessary. Prior to each experiment, overnight cultures were adjusted to an optical density at 600nm (OD_{600}) of 2.0 and if required, mixed in a 1:1 ratio, before being back-diluted 1:100 in fresh LB medium. These cultures were incubated in 14 ml round-bottomed polystyrene test tubes (Falcon, Corning) on a carousel style rotary wheel (40 rpm) at 30°C.

METHOD DETAILS

Bacterial strain engineering

Standard methods were used for DNA manipulations and molecular cloning.[93] All genetically engineered strains were verified by PCR, Sanger sequenced by Microsynth AG, and analyzed using SnapGene (v. 4.3.11). Genetic engineering of *V. cholerae* was done by natural transformation followed by FLP recombination (TransFLP),[68,94,95] tri-parental mating,[79] or allelic exchange using

Please cite this article in press as: Otto et al., Interactions between pili affect the outcome of bacterial competition driven by the type VI secretion system, Current Biology (2024), https://doi.org/10.1016/j.cub.2024.04.041

the counter-selectable plasmid pGP704-Sac28.[81] For creating red fluorescent strains, the optimized *mCherry*$_{op13}$ gene[96] was used as a template.

Bacterial competition assays

The relative competitive index (RCI) of predator strains was evaluated in co-culture experiments using the specified predator-prey strain pairs. Cultures were typically grown for 6 h, followed by a wash step in PBS and subsequent vortexing for 10 min at maximum speed to disperse the aggregates into single cells. Right after dispersion, cells were serially diluted in PBS, and both prey and predator strains were counted on selective antibiotic-containing plates.

The predator RCI was calculated as the predator-to-prey ratio at the end of the experiment, divided by the starting ratio: $RCI = [N_{predator}(t = 1)/N_{prey}(t = 1)] / [N_{predator}(t = 0)/N_{prey}(t = 0)]$, where $N(t = 1)$ is the numerical density (N) at the end of the experiment and $N(t = 0)$ is the one at the start.[35,58] Throughout, we mainly consider the natural log-transformed RCI, denoted as log RCI.

The RCI of strains solely carrying the antibiotic/fluorescent markers was determined in co-culture experiments using A1552Δ*lacZ* as the reference strain, following previously established methods.[97] Strains were competed in fresh LB medium in the absence of antibiotics for 8 h. At the beginning and end of the experiment, the proportions of blue (antibiotic/fluorescent marker strain) and white (reference strain) colonies were counted through serial dilution in PBS, followed by plating on LB agar plates supplemented with 5-bromo-4-chloro-3-indolyl β-d-galactopyranoside (X-gal; 40 μg ml^{-1}). Subsequently, the RCI was calculated as above, but comparing blue-to-white ratios.

Bacterial imaging through light microscopy

To visualize aggregates, overnight cultures were back-diluted, as mentioned previously, and were grown for 4 h. The cells were immobilized by mounting them on slides coated with an agarose pad (1.2% wt/vol in PBS), covered with a coverslip, and imaged immediately using a Zeiss Axio Imager M2 epifluorescence microscope with an AxioCam MRm camera, controlled by Zeiss Zen software (ZEN 2.6 blue edition). Images were captured using a Plan-Apochromat ×100/1.4-NA Ph3 oil objective illuminated by an HXP120 lamp and were analyzed and prepared for publication using Fiji.[82] To stain lysed cells, the agarose pad was supplemented with 0.5 μM SYTOX Blue Nucleic Acid Stain (Thermo Fisher Scientific) as previously described.[59]

Bacterial aggregation assay

Aggregation assays were conducted following the established protocol.[51] Bacteria were grown for 6 h, then left to settle for durations specified in the figure legends. The level of aggregation was determined by measuring the OD_{600} before and after vortexing (vortexed at maximum speed for approximately 5 sec), during which the settled aggregates were resuspended into the solution.

Computational model development and testing

An agent-based model was developed on a lattice, grounded in physical principles and incorporating the key biological components of the system. The focus was directed towards the events subsequent to the production of T4Ps and T6SS, precisely from the 3-hour mark in the experiments. Stochastic simulations of the model were conducted, employing experimentally measured parameter values whenever available (Table 1). The model was simulated on a lattice in both two and three dimensions, with primary emphasis placed on the three-dimensional case in the main text, owing to its closer approximation to real-world conditions (see Figure S5B for examples of two-dimensional simulations). In the three-dimensional case, each cell sits on a site of a body-centered cubic lattice. The following paragraphs outline the fundamental components of the model.

Division

In our model, a cell can divide with rate k_{div}, matching the experimentally measured value, if at least one of its neighboring sites on the lattice is empty. The offspring is identical to its parent cell and is placed on a randomly chosen empty neighboring site. In our experiments, the cell division rate was determined to be $k_{div} = 1.58h^{-1}$. The growth rate was calculated using the formula $k_{div} = \log[(OD_2/OD_1)/(T_2 - T_1)]$, where OD represents the optical density and T represents the incubation time. The values 1 and 2 correspond to the start and end, respectively, of the linear portion of the optical density curve of the wild-type *V. cholerae* grown under the specified growth conditions. Exact measurements can be found in the source data file.

Transport

In our experimental setup, bacteria are placed in test tubes and subjected to agitation through rotation. This is relevant due to the turbulent flow observed in the natural habitat of *V. cholerae*, predominantly in oceans, estuaries, and rivers.[98–100] In a turbulent regime, passive transport by the medium can be modelled by eddy diffusion. In addition, *V. cholerae* bacteria can actively swim, but the agitation of the medium prevents any substantial gradient that might bias their motion via chemotaxis or quorum sensing. Thus, their active swimming motion may also be simply modelled by diffusion.[101] We therefore model transport through an effective diffusion coefficient D, which incorporates both passive and active transport.

Eddy diffusion coefficients are challenging to measure as they are contingent on local flow velocity and the sizes of eddies.[100] However, they are usually significantly larger than the molecular diffusion coefficient $D_{mol} = 5 \times 10^{-13} m^2 s^{-1}$, obtained via the Stokes-Einstein equation $D_{mol} = kT/(6\pi\eta R)$, where k is the Boltzmann constant, $T = 300\,K$ is the absolute temperature, $\eta = 8{\times}10^{-4} Pas$ is the dynamic viscosity of water and R denotes the effective radius of bacteria, i.e. the radius of a sphere with the experimentally-measured volume of a wildtype *V. cholerae* bacterium.[102] Active diffusion coefficients associated to swimming can be expressed

from the properties of bacterial swimming trajectories,[101] and are of the order of $10^{-11}m^2s^{-1}$ for *Escherichia coli* run and tumble motion. In our simulations, we adopted a phenomenological value of $D = 3 \times 10^{-12}m^2s^{-1}$, which was found to reproduce the experimentally observed aggregate formation in the absence of killing by T6SS. However, we note that there is uncertainty on this value. For instance, *V. cholerae* was recently found to swim faster than *E. coli*,[103] which could yield a larger effective diffusion coefficient. We found that an increased diffusion coefficient mainly accelerates cluster formation and results in aggregates that are somewhat more spherical after 1 hour (Figures S5C and S5D), but does not affect our main results. It also makes simulations more computationally demanding. Importantly, previous work had shown that aggregate formation is maintained in non-motile *V. cholerae*.[51]

In addition to individual bacterial cells, aggregates of bacteria bound by T4P interactions may also diffuse as a single unit. We include this effect for completeness, but it is worth noting that there are various possible detailed choices for its implementation (Are neighboring non-bound bacteria pushed by a moving aggregate? Are they pulled by it? Can aggregates break into large blocks? Can they merge? Is their effective diffusion coefficient the same as for single bacteria? For simplicity we answered yes, no, no, yes and yes to these questions). Given these complications, simulations were also conducted without considering any aggregate diffusion. Figure S5E demonstrates that simulations with and without aggregate diffusion yield qualitatively similar results regarding cluster composition in the case of diverse T4Ps, and we also obtained similar results in other cases. Therefore, this effect or its variants do not influence our conclusions.

In practice, in our lattice model, diffusion is implemented via bacteria hopping randomly to any free neighboring site, with a rate k_{hop} which is derived from the diffusion coefficient: $k_{hop} = dD/(2zR^2)$, where $d = 3$ is the dimension considered (3D here), $z = 8$ is the number of nearest neighbors per site in the body-centered cubic lattice, and R is the effective radius of a bacteria (see above). Since each site has 8 neighbors, the total hopping rate of a bacteria is $8k_{hop}$, if all its neighboring sites are free.

Interactions via T4P

The effect of T4Ps is modelled as an attractive interaction between neighboring bacteria on the lattice. Considering that the T4P of prey and predators may differ, three types of interactions are considered, each with potentially different binding energies: E_{prey} between two prey cells, $E_{predator}$ between two predators and E_{cross} between a prey and a predator. Importantly, these interactions have an impact on the ability of individual bacteria to diffuse. Qualitatively, a bacterium bound to many others will be less likely to move away, due to the requirement of detaching from its neighbors. To model this, we assume dynamics that ensures detailed balance for these moves.[104] The hopping rate of a prey to any free neighboring site is $nk_{hop}\exp(-n_{prey}E_{prey} - n_{predator}E_{cross})$ where k_{hop} is the baseline hopping rate of a freely diffusing bacterium, while n is the number of free neighboring sites, n_{prey} the number of neighboring prey and $n_{predator}$ the number of neighboring predators (note that $n + n_{prey} + n_{predator} = z$). A similar formula can be written for the hopping rate of a predator.

We are not aware of precise measurements of the binding energy associated with T4Ps in *V. cholerae*. Note that force measurements exist, but obtaining an interaction energy is challenging.[34,105] Because T4P binding energies are not precisely known, we varied them in our simulations.[106] The first key point is that they need to be strong enough to ensure effective aggregation of prey and predator separately, as observed in the experiments. Indeed, as shown in Figure S5F, in a system where there is only this attraction and transport (no division, no killing), aggregation occurs above $2kT$ in 2D and $2.5kT$ in 3D at the densities we considered, where kT is the scale of thermal fluctuations (k being the Boltzmann constant and T the absolute temperature). These thresholds correspond to the liquid-gas phase transition in a lattice fluid, both in 2D[107] and 3D,[108] and they are in good agreement with theoretical mean-field calculations. Therefore, we choose E_{prey} and $E_{predator}$ above these thresholds. Experimental results are well matched for energies not exceeding a few kT. Thus, in practice we take $3kT$. Then E_{cross} should be either the same for matching T4Ps, or smaller otherwise, and we vary it in the latter case. Here, we simply model T4P binding with effective binding energies. However, T4Ps are active systems, especially in the presence of PilT, which is deleted here. More detailed modelling of these active processes has been performed in other works.[109–111]

Killing by T6SS

A predator can kill a neighboring prey at rate k_{kill}. Once a killing event occurs, the prey enters a lysing state, and is removed from the system at a certain rate k_{lysis}. For simplicity, it is assumed that, while lysing, a prey moves and interacts with other bacteria in the same way it did before being killed. However, it is unable to divide. The values $k_{kill} = 6.25h^{-1}$ (total firing rate $k_{fire} = 50h^{-1}$ divided by the 8 possible firing directions in the lattice) and $k_{lysis} = 1/75\ min^{-1}$ (mean lysis time = 75 minutes) were chosen based on the ranges found in the literature[64,65] (Table 1).

Initial density

In experiments, the average initial inoculum comprises 10^7 bacteria in 2 mL of solution, and the induction of T4Ps and T6SS production continues for 3 hours until the observation of aggregates at the 3.5-hour time point (Figure 1E). Therefore, assuming exponential growth at a rate $1.58h^{-1}$, the density at the onset of aggregation is estimated to be around 10^9 bacteria per mL. In our 3D simulations, a 40×40×40 body-centered cubic lattice (comprising 2 sites per unit cube) was considered, and the initial population consisted of 100 bacteria (comprising half prey and half predators as in the experiments), resulting in approximately $2\times100/\left(40\times4R/\sqrt{3}\right)^3 \approx 10^9$ bacteria per mL, where R represents the effective radius of a bacterium (see above).

Simulation methods

The simulations are conducted using a kinetic Monte Carlo algorithm.[104] Time is discretised with a timestep chosen to ensure that it is unlikely that substantially more than one event occurs within a step, typically on the order of 1 microsecond. Periodic boundary conditions are applied.

Please cite this article in press as: Otto et al., Interactions between pili affect the outcome of bacterial competition driven by the type VI secretion system, Current Biology (2024), https://doi.org/10.1016/j.cub.2024.04.041

Assortment: Characterization of mixing within aggregates

Denoting prey by A and predators by B, we define assortment as $n_{AB}/n_{AB,max}$ where n_{AB} is the number of adjacent prey-predator pairs, while $n_{AB,max}$ is its maximum expected value, obtained if all bacteria were randomly mixed and in the bulk of an aggregate. The latter is $n_{AB,max} = n_A \times 8 \times n_B/(n_A + n_B)$, namely the number of prey, times the number of neighboring sites it has in the lattice (8), times the probability that a neighboring site is occupied by a predator, assuming that all neighboring sites are occupied (which is the case in the aggregate bulk), and that prey and predators are randomly mixed. Note that lysing prey are counted as prey in the calculation of assortment.

Bioinformatical analysis and phylogeny

Vibrio spp. genomes used in this study are detailed in the key resources table. Any genomes that were not previously annotated were annotated using the prokaryotic genome annotation pipeline (PGAP, 2022-10-03. build6384).[83] To reconstruct the evolutionary history of the studied strains, we first assembled their pangenome along with a *V. mimicus* strain as an outgroup. We used PPanGGOLiN (v. 1.2.74)[84] and provided both sequences and annotation to the program, while the rest of the parameters were set to default. 1186 core genes were identified across the strains. We provided the core genes to Modelfinder[112] to assess gene-specific optimal evolutionary models. Finally, the phylogenetic reconstruction was performed using iqtree2 (v. 2.2.0).[85] *V. mimicus* was set as the outgroup and 100 bootstraps were computed in iqtree2. Nodes with bootstrap values under 60 were collapsed using the collapseUnsupportedEdges function in the ips package (v. 0.0.11, R environment).[86,87] GC content was analyzed by SnapGene (v. 4.3.11).

T6SS clusters in each genome were identified through blast analysis. A nucleotide database was created using all the studied genomes by employing the makeblastdb command (v. 2.12) with default parameters. The conserved flanking genes for each T6SS cluster were selected based on their known arrangement. These genes were then used as boundaries to identify the T6SS clusters within the genomes. The A1552 sequences were used as query sequences (blastn, default parameters, e-value 1e-10) to detect each respective cluster in the other strains, including the large cluster and auxiliary clusters 1 to 3. For auxiliary clusters 4 and 5, we utilized the same approach using the sequences from *V. cholerae* strain S12[40] and *V. cholerae* strain BC1071,[41] respectively, as query.

To assess the different families and subfamilies of individual clusters, we selected cognate immunity proteins of E/I protein pairs for each cluster. These immunity protein sequences were then aligned using muscle (v. 5.1.osx64, default parameters). The hierarchical clustering and the identity matrices for each T6SS cluster were computed in an *R* environment (v. 4.2.1), using the filter.identity function (cutoff = 0.3) in bio3d package (v. 2.4-4). Heatmaps were then visualized with the pheatmap function (v. 1.0.12).

The PilA nucleotide and protein sequences were collected based on the genome annotations for each strain. A phylogenetic tree of the *pilA* nucleotide sequences of the studied strains was reconstructed using iqtree2 (v. 2.2.0), and its statistical relevance was asserted with 100 bootstraps. The best model of evolution was determined using ModelFinder. Nodes with bootstrap values below 60 were collapsed using the collapseUnsupportedEdges function. The protein sequences were aligned using muscle, and the identity matrix was obtained in the *R* environment through the seqidentity function in the bio3d package (v. 2.4-4). The resulting heatmap was visualized with the pheatmap function (v. 1.0.12).

QUANTIFICATION AND STATISTICAL ANALYSIS

All data represent the outcome of three independent biological experiments, demonstrating consistent results. Bar graphs illustrate the mean value, with error bars denoting the standard deviation. For scatter dot plots, lines represent the mean value. Statistical analyzes were conducted using GraphPad Prism (v. 9.1.2). Differences were assessed using one-way ANOVA ($\alpha = 0.05$) and adjusted for multiple comparisons by the Tukey post hoc test or by a two-tailed Student's t-test ($\alpha = 0.05$), when appropriate.